Stern-Gerlach Resonance Polarimetry

Richard Talman
Laboratory of Elementary-Particle Physics
Cornell University
June 1, 2016

Abstract. There have been recent proposals to measure the electric dipole moment (EDM) of fundamental charged particles, especially proton, deuteron, and electron. Any non-zero EDM would imply violation of both time reversal (T) and parity (P) conservation and could help to account for the particle/anti-particle imbalance in the present day universe.

For this measurement the particles circulate in a storage ring with their spins "frozen", for example parallel to their velocities. Polarimetry is required both to stabilize the frozen spin operation and to measure the EDM-induced precession. The efficiency of currently available polarimetry, especially for electrons, is too low to permit phase-locked loop stabilization of the beam polarization. A new, as yet unproved "resonant, Stern-Gerlach polarimetry" directly measures the magnetization of bunches of polarized electrons, or other charged particles.

To confirm the practicality of resonant polarimetry, first proposed by Derbenev in 1993, and resurrected by Talman in 2012, various tests have been proposed, but not yet performed. This paper is intended to clarify various issues, both experimental and theoretical, and to propose a multi-step plan for developing Stern-Gerlach polarimetry.

A first, proof-of-principle, test using polarized electrons in the extraction line of the CEBAF recirculating linac at Jefferson Lab is proposed. The goal of the test would be to demonstrate measureably large excitation of a room temperature copper cavity by a beam of transversely polarized electrons. Slanted, off-axis beam passage through a rectangular TE_{202} mode resonator largely defeats a source of destructive interference that has discouraged previous attempts. Sensitivity to magnetic end fields of the cavity is to be investigated using DC magnets.

Once the resonance has been successfully and inexpensively demonstrated, application of Stern-Gerlach resonance for polarimetry can be developed and greatly improved by using high Q superconducting cavities and sensitive low temperature readout instrumentation.

Contents

1. Proposed Stern-Gerlach polarimetry development plan

This section is closer to being conclusions than it is to being a conventional introduction. Results from later in the paper are surveyed with brief explanation, with details deferred to later sections. The final section, titled "Recapitulation and conclusions", explains why this paper is more nearly a development plan for Stern-Gerlach polarimetry than it is an exposition of theoretically possible polarimeter performance.

A practical first step toward the development of Stern-Gerlach polarimetry would be a demonstration of resonant excitation of an RF cavity by a polarized beam. A high-Q cavity will be resonantly excited to an amplitude proportional to the beam current multiplied by the beam polarization. Prospects for this technique were discussed most recently in early 2016 at a three day Jefferson Lab workshop on the subject. The workshop was attended by researchers from Jefferson Lab, Cornell, Juelich-COSY and Bonn-ELSA labs in Germany, and others, and a tentative collaboration was established.

Because of the large electron magnetic moment, a polarized electron beam, either from a linac or in a storage ring, is favored over protons or deuterons for the first demonstration of Stern-Gerlach polarimetry. As well as its potential value for polarimetry, the physics of magnetic moments moving relativistically through a resonant cavity is itself of fundamental importance.

Resonant polarimetry was first proposed in 1993 by Derbenev[**1**]. The expected cavity response was calculated by Conte et al.[**2**] in 2000. An experimental test at MIT Bates Lab was proposed[**3**] in 2001, but not performed. This may have been because, at that time, the interaction between polarized beam with a resonant cavity was controversial (as it still is, but to a far lesser extent). The importance of this controversy, and the way it can be resolved forms a significant fraction of this paper. The resonant polarimeter idea was resurrected by Talman in 2012, motivated by the need to control a "frozen spin" polarized electron or proton beam, appropriate for measuring their electric dipole moments.

The original Conte et al. Stern-Gerlach resonator configuration is illustrated on the top left of Figure 1. The configuration for the proposed CEBAF test is shown in the top right of the figure. The lower figure shows a more complicated, dual resonator, configuration that would be appropriate for "transparent" inclusion in a storage ring EDM experiment.

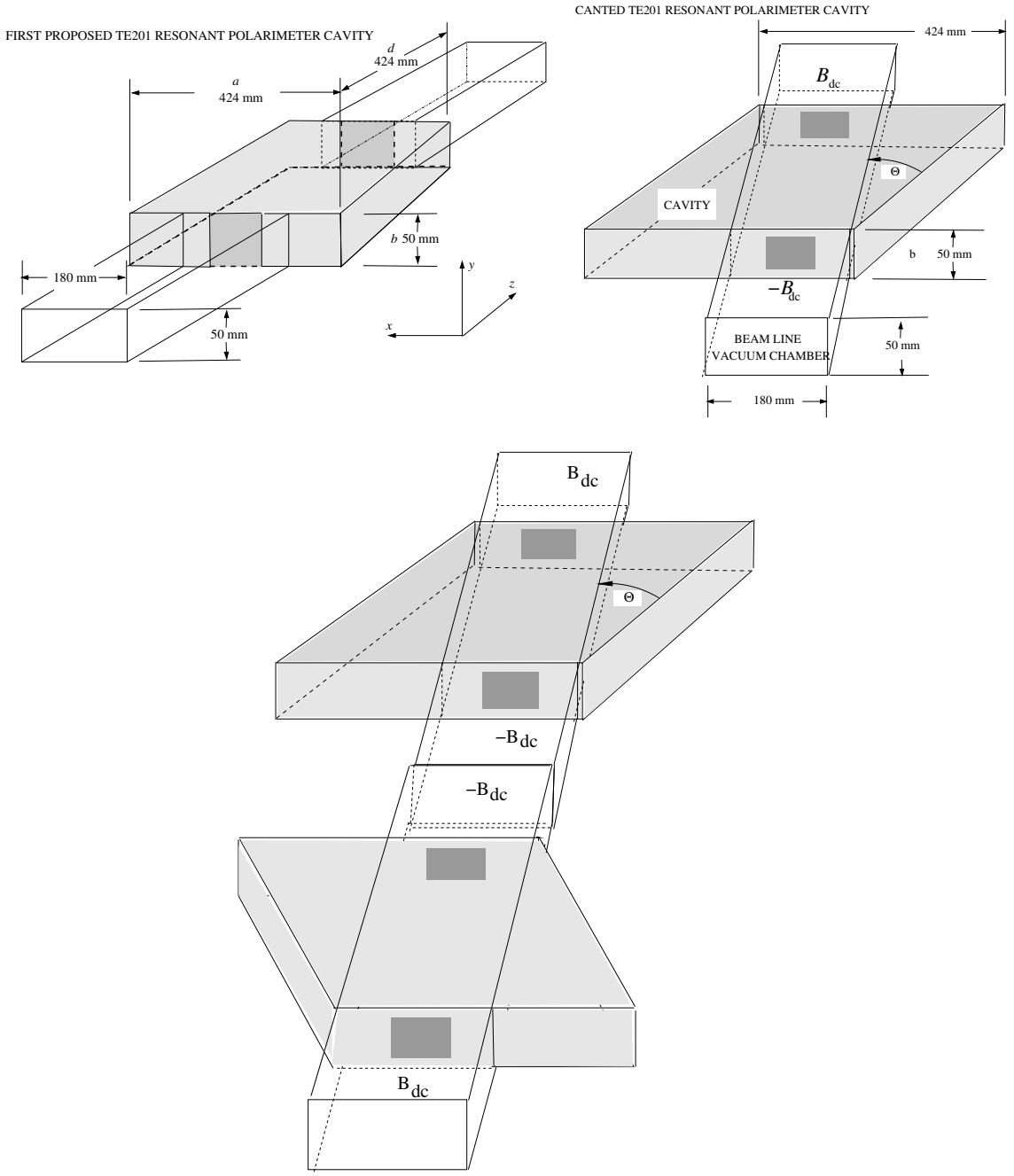

FIGURE 1. Stern-Gerlach polarimeter cavity insertions in polarized beam lines; on-axis beam top left; skew beam with external DC magnetic fields top right; skew incidence with dual resonators with DC magnetic fields at the bottom. DC magnet coils are not shown. The cavity dimensions have been adjusted for a possible test in the CEBAF extraction line; they are not matched to a possible storage ring test described later in this paper.

The resonator is a conventional, rectangular, TE mode cavity, with standard, on-axis passage of the beam through the cavity. In 2008, C. Tschalaer[**4**] showed theoretically that this configuration is guaranteed to give zero Stern-Gerlach cavity excitation. My explanation, consistent with Tschalaer's, led to the configuration shown in the upper right of Figure 1. The slanted trajectory through the cavity overcomes much of the destructive interference present with on-axis passage. The complete cancellation for on-axis passage is embarrassingly elementary:

Accelerating cavities use TM modes, with the acceleration being due to longitudinal cavity electric field. To the contrary, magnetic moment detection requires TE modes, to take advantage of their longitudinal magnetic fields. In the present context the essential difference between TM and TE modes is the boundary conditions on the entrance and exit sufaces of the cavity. In both cases the electric field has to be normal to the surface, and the magnetic field parallel to the surface. In TM modes, electric field normal to entrance and exit surfaces is ideal for charged particle acceleration, since longitudinal electric field is what is essential for applying a longitudinal force to the particles.

But it is longitudinal magnetic field that enables a magnetic moment to transfer energy to the cavity. This calls for TE cavity modes. By the boundary condition already mentioned, TE modes necessarily have stationary nodes for longitudinal magnetic field at both entry and exit. On entering the cavity, at no matter what phase (relative to the cavity oscillation) the particle encounters a purely transverse magnetic field. Along the particle path the longitudinal magnetic field first increases from zero and then decreases symmetrically back to zero at the exit. Any work done during the field-increasing interval is cancelled during the field-decreasing interval, and there is no net cavity excitation. For Stern-Gerlach resonance this rules out on-axis passage through any cavity, cylindrical or rectangular.

To overcome this cancellation the resonator can be canted as shown on the top right in Figure 1. Calculation of cavity excitation is illustrated in Figure 2. The arrows in these figures represent magnetic field lines. The cavity walls are not shown. Figure (a) shows a TE_{201} mode. As just explained, on-axis beam passage of a polarized beam through this (or any) cavity would produce zero excitation.

Skew injection at (quite extreme) 45 degree angle is indicated by the slanted line. As it happens, direct calculation gives exactly zero cavity excitation also in this case. It is because the actual waves making up the TE_{201} mode are traveling at exactly ± 45 degrees. As with 0 degree entry, this is an exceptional case.

(Incidentally, the vanishing of integrated body force within the cavity does not guarantee the exact absence of total cavity exitation; the effect of end fields must also be included. Integration of the work done by a longitudinal Stern-Gerlach force acting over the interior of the cavity bounded by discontinuous edges at the ends includes, to a first approximation, a contribution from the end fields. With gentler, less abrupt, edges, the work done from "half-way up" the entrance field to "half-way down" the exit is already approximately included. When approximated by an idealized, internal to cavity calculation, what is not included is the perturbative effect of the fields bulging

out from the resonator into the adjacent waveguides. The influence of end fields remains controversial, and requires evaluation going beyond what is contained in this paper.)

A less extreme, $\Theta = 26.57$ degree skew entry is illustrated in Figure 2 (c). The (x, z) coordinates have been converted to dimensionless angles $(\tilde{x}, \tilde{z})$ to simplify calculations. Dimensions are given in the figure on the right. (Because these dimensions have been somewhat altered to match the proposed CEBAF test, they may not be quite consistent with other calculations later in the paper.) In this case there is a "race" between particle traveling at speed V in the skew direction and a wave front moving parallel to the z-axis at waveguide phase velocity v_g (which is $\sqrt{2}\,c$ in this case). For maximum excitation the phase difference at the exit would be $\pm\pi$ (or any odd multiple) since this would correspond to perfect longitudinal magnetic field reversal during transit. A penalty function $\mathcal{P}(\Theta)$, where Θ is the skew entrance angle, expresses the excitation fraction imposed by the geometry. In the TE_{202} case shown, the penalty function is later calculated to be $\mathcal{P}(26.57^\circ) = 0.25$, meaning the exitation is $1/4$ of the maximum possible.

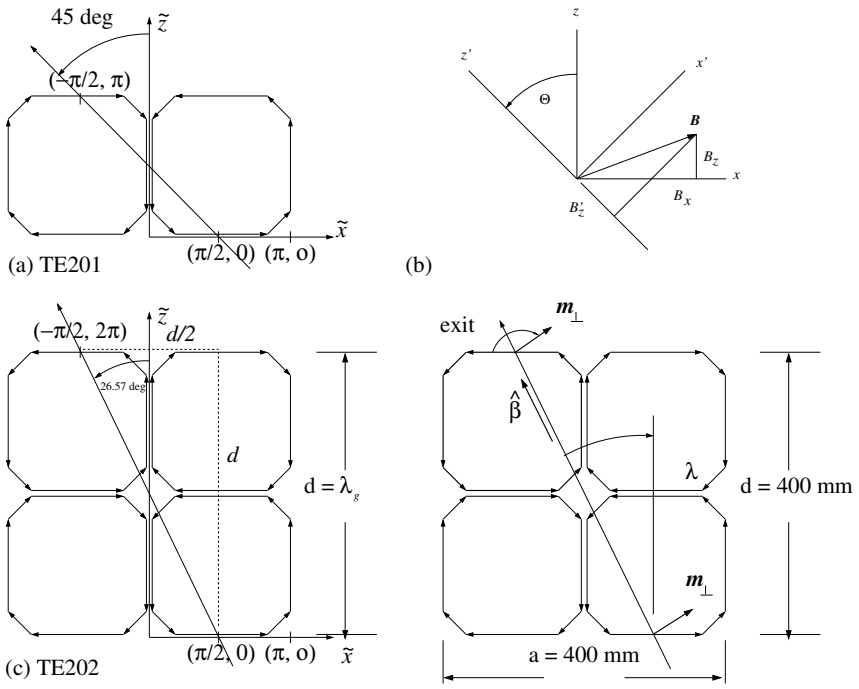

FIGURE 2. (a) TE_{201}, $\Theta = 45^\circ$ case. Tildes indicate dimensionless coordinates. Arrows are magnetic field lines. Cavity walls are not shown. In this TE_{201} case $\mathcal{P}(45^\circ) = 0$ because the longitudinal Stern-Gerlach force vanishes identically on this trajectory. (b) Erect and skew coordinate frames. (c) For the TE_{202}, $\Theta = 26.6^\circ$ case, $\mathcal{P}(26.6^\circ) = 0.25$. This result follows from the difference between wave phase velocity v_p and particle velocity V.

There is yet another source of destructive interference that suppresses cavity excitation by the passing magnetized beam bunch. In a 2015 report, Tschalaer[**6**] shows that, integrating from a point of zero magnetic field before the cavity to a point of zero magnetic field after the cavity, the recoils occurring within the cavity are cancelled by recoils in the external end fields of the cavity as shown at the bottom of Figure 1. DC magnetic field regions adjacent to the RF cavity overcome the cancellation, by moving the zero magnetic field points to remote locations that cannot influence the cavity excitation. Transient coupling effects in the cavity are not included in the Tschalaer formulation.

The configuration shown at the bottom of Figure 1 has been further complicated by the presence of two, rather than one, cavity. The four DC magnetic bends form a "chicane" whose amplitude can be varied with only a very small change in orbit circumference, but with no change in closed orbit outside the chicane region. This degree of complexity is likely to be required for successful Stern-Gerlach polarimetry in a storage ring, but is unnecessary for an initial CEBAF test.

Cavity excitation can be expressed as energy deposited per beam particle passing through the resonator. There are three important cavity excitations. The first is direct excitation $\Delta\mathcal{E}^{eTM,\max}$ of the nearest (in resonance frequency) TM mode, excited by the passage of the charge itself. This is the dominant "background". Because of the high Q_r-value and the frequency difference Δf, this excitation can be filter suppressed by a small factor, $f/(Q_r\Delta f)$. Even so, this excitation will dominate unless the $Q_r\Delta f$ factor is large. $\Delta\mathcal{E}^{m_\parallel TE,\max}$ and $\Delta\mathcal{E}^{m_\perp TE,\max}$ are "foreground" resonator excitations due to longitudinal and transverse beam polarization components, at the Stern-Gerlach resonator frequency $f_{\rm SG}$, to which the excitation frequency is tuned. As with nuclear magnetic resonance, the resonance can be detected by scanning the beam energy, which scans the spin tune through Stern-Gerlach resonance.

Theoretical values for these three excitations are expressed in the following ratios:

$$\Delta\mathcal{E}^{eTM,\max} : \Delta\mathcal{E}^{m_\parallel TE,\max} : \Delta\mathcal{E}^{m_\perp TE,\max} = eE_\parallel : k\gamma_{_V}\mu_e^*\mu_0 H_\parallel : \mathcal{P}(\Theta)\, k\gamma_{_V}^2\mu_e^*\mu_0 H_\parallel. \quad (1)$$

Here e is electron charge, k is laboratory frame vacuum wave number, and μ_e^* is electron magnetic moment. $E_\parallel$ is the resonator electric field in a TM resonator mode; $H_\parallel$ is the resonator magnetic field in a "matching" TE mode resonator mode. Dependence on beam relativistic factor $\gamma_{_V}$ is of critical importance, expecially for the response to transverse polarization. We have pretended that longitudinal magnetic field $H_\parallel$ (measured in A/m) is given in terms of $E_\parallel$ (measured in V/m) by $H = E_\parallel/Z_0$ where the value of free space impedance Z_0 is 377 ohms, even though this is strictly true only for transverse fields in free space. This means that, for simplicity, we ignore the detail that, for longitudinal waveguide fields, the impedance is somewhat (but not very) different from Z_0. The purpose for this approximation has been to make $E_\parallel$ appear as a common factor in Eqs. (1). This is convenient for estimating relative excitations. Noting that $\mu_0/Z_0 = c$, a convenient physical constant for the magnetic vs electric comparison is the length

$$\frac{\mu_e^*}{ec} = \frac{0.928\times10^{-23}\,\mathrm{J/T}}{(1.602\times10^{-19}\,\mathrm{C})\times(2.9979\times10^{8}\,\mathrm{m/s})} = 1.932\times10^{-13}\,\mathrm{m}. \quad (2)$$

Dimensionally this length factor cancels the inverse length dimensionality of k in Eqs. (1). Along with laboratory length d of the resonant cavity, this factor dominates the comparison of "background" electron charge source "e" to the "foreground" magnetic dipole source strength $\mu_e^*/(cd)$. A basic, dimensionless, Stern-Gerlach/electric excitation ratio is

$$\frac{\text{Stern} - \text{Gerlach}}{\text{electric charge}} = \frac{\mu_e^*}{ec}\frac{2\pi}{\lambda} \approx 2.0 \times 10^{-12} \tag{3}$$

where a typical value for the cavity length has been used to produce a typical k value. This confirms our impression that Stern-Gerlach forces are very weak. Most of the present paper amounts to producing factors that, taken together, enhance the Stern-Gerlach "foreground" signal (relative to the direct electric charge "background" signal) by the 12 or so orders of magnitude basic ratio.

TABLE 1. Suppression and enhancement factors for a proposed test of Stern-Gerlach polarimetry the polarized electron in the extraction line of the CEBAF recirculating linac beam at Jefferson Lab. The Stern-Gerlach cavity response to magnetic dipole moment μ_e^* is superimposed on the direct response due to electron charge e. This table provides factors (either suppression or enhancement) contributing to the extraction of the Stern-Gerlach signal. The final column points to the section containing the primary discussion of the factor.

quantity	symbol	suppression/ enhancement	enhancement factor	section number	figure or Eq. number
physical constants		$\mu_e^*/(ec)$	$1.932 \times 10^{-13}\,\text{m}$	S1	Eq. (2)
resonant wave number	k_r	$2\pi/\lambda_r$	$10.5/\text{m}$	S1	Eq. (3)
skew penalty	$\mathcal{P}(\Theta)$		0.25	S7.2	FIG 2
beam energy (MeV)	γ_V^2	$(4000/0.511)^2$	1.6×10^7	S4	Eq. (87)
frequency sensitivity	$Q = f/\Delta f$	10^4	10^4	S5.2.1	FIG 7
cavity mode suppression	TE/TM	$1/\sigma_{\Theta_y}, 1/\sigma_{AB}$	10^2	S6	FIG 4
polarization reversal	2 kHz		10^2	S6	

Table 1 lists "suppression" factors causing the Stern-Gerlach signal to be small, as well as enhancement factors to be employed in the extraction of the S-G signal. The ratio of physical constants of Eq. (3) is the main suppression factor needing to be overcome. There is also a minor suppression factor $\mathcal{P}(\Theta)$ referred to as the penalty for skew passage of the beam through the resonant cavity.

The largest enhancement factor is the γ_V^2 factor for transverse polarization. For 1 GeV electrons, $\gamma_V^2 = 4 \times 10^6$ which, multiplied by $\mathcal{P}(\Theta) = 0.25$, produces 2×10^{-6} as an estimated ratio of magnetic over electric excitation. Without further enhancement, even the transverse signal remains small compared to the direct charge exitation. The discovery that the γ_V^2 factor had been erroneously included for on-axis beams is perhaps what terminated previous investigations? The canted resonator configuration largely restores the validity of retaining the γ_V^2 factor, though reduced by penalty factor $\mathcal{P}(\Theta)$.

The effect of fringe fields at resonator ends has been neglected, so far. Beam interaction with end fields is certainly capable of altering the cavity excitation. In passage of a charge through a conventional RF cavity the end field accelerations give only a fractionally small effect, especially if the transverse aperture dimensions are small. As explained previously the excitations given in Eqs. (1) account for the work done from half-way up the entrance transition into the resonator, to half-way down the exit. What is not included is the perturbative effect of the bulging out of the fields into the adjacent waveguides.

Unfortunately fractionally small end field acceleration in electric acceleration does not guarantee comparably small fractional effect in end field magnetic acceleration. This remains controversial. It has not been ruled out theoretically that there is a powerful overall magnetic conservation law, according to which vanishing of the orbit path integral $\int B_{\parallel}(z)\,dz$ over a range from well before to well after the cavity, would cause the cavity excitation to vanish identically. In the skew geometry, because the end fields are also not skew to the cavity, this integral would not, in fact, vanish. This calculation is difficult, however, and has not yet been performed. The end field effect will introduce a further "fringe-field" penalty function $\mathcal{P}_{\rm FF}$ whose value can be guessed to be comparable to the body field penalty $\mathcal{P}$.

1.1. Sequence of tests, starting at CEBAF. The proposed initial test of Stern-Gerlach polarimetry at CEBAF is described in some detail in Section 6. This test is expected to be the first in a long and ambitious plan for developing and refining S-G polarimetry. The present section sketches out a possible sequence of developments, more or less in order of increasing difficulty and cost.

The Stern-Gerlach excitation is weak, in absolute terms, and also weak relative to direct excitation. Nevertheless, even under worst case assumptions, with modern signal detection and cavity design and readout, Stern-Gerlach polarimetry can be expected, eventually, to become practical. Once the Stern-Gerlach resonance has been successful demonstrated in an inexpensive proof-of-principle test, its performance for polarimetry can be greatly improved. For maximum sensitivity, Stern-Gerlach polarimeters will use ultra-high Q superconducting resonant cavities, with strong higher mode damping, and highly sensitive instrumentation readout. Unfortunately these developments can be expected to be expensive and to require long development times. This is why the most promising, least difficult test has to be identified first.

It is essential to make a plan that will lead from success to success, while minimizing the expense and effort at each stage. A sequence of such tests is listed next, more or less in the order from least to most ambitious.

(1) **Instrumentation-free, betatron-readout, unloaded Q_r test:** The quickest possible test of the principle of Stern-Gerlach polarimetry would be completely passive, with no cavity instrumentation, nor higher mode damping, needed whatsoever. The TE_{202} cavity mode, once it has rung up resonantly in response to the Stern-Gerlach force, will have non-zero electric field component E_y and horizontal magnetic field B_x. These fields oscillate at the Stern-Gerlach frequency $f_{\rm SG}$ and deflect the beam vertically at that frequency. Standard

beam position monitor betatron motion detection, with frequency domain filtering by spectrum analyser, can detect the betatron motion driven by the resonant cavity with exquisite sensitivity, and with negligible beam loading of the cavity. There is ample frequency domain selectivity to distinguish Stern-Gerlach response from direct charge response for two reasons: the TM and TE resonant frequencies are separated and there is a large (and controllable) frequency difference between (harmonics of) the circulation frequency and the magnetization frequency. Preliminary estimates indicate that the resulting beam deflection will be detectible by scanning the spin tune slowly through the Stern-Gerlach resonance frequency.

With N_e electrons per bunch, repetition frequency f_0, resonator quality factor Q_r, the cavity excitation gain and loss for transverse polarization are given by

$$P^{\rm SG} = f_0 N_e \mathcal{P}(\Theta)\gamma_V^2 \mu_e^* \mu_0 H_\parallel, \quad \text{and} \quad P_{\rm loss} = \frac{2\pi f_{\rm SG}}{Q_r}\,\mu_0 H_\parallel^2\,\frac{abd}{8}. \tag{4}$$

In equilibrium $P^{\rm SG} = P_{\rm loss}$. Equating these expressions and solving for the magnetic field yields equilibrium (oscillating at frequency $f_{\rm SG}$) magnetic field

$$B_\parallel = \mu_0 H_\parallel = \frac{N_e Q_r}{10^{16}}\left(\frac{f_0}{f_{\rm SG}}\,10^{16}\mathcal{P}(\Theta)\gamma_V^2\mu_e^*\mu_0\frac{8}{2\pi a\,b\,d}\right). \tag{5}$$

The factor 10^{16} has been multiplied and divided only for discussion purposes, to make 10^{16} be a convenient tentative value for the N_eQ_r product. A sample numerical evaluation of the product in parenthesis yields $4\times10^{-8}\,$T. This oscillating field applies an (approximate) deflection $\Delta\theta \approx B_\parallel d/(pc/e)$ to the beam. In a 1 GeV storage ring with typical beta function value of 1 m, the resultant vertical displacement would be approximately $5\times10^{-9}\,$m for $N_eQ_r = 10^{16}$.

According to Inoue et al.[**7**][**8**], for a 1.3 GeV electron beam with 10^{10}e/bunch at bunch frequency of about 1 Hz, (or, presumeably, about 10^4e/bunch at 1 MHz), the voltage response of a sensitive resonant beam position pick-up is about 3μV/nm, with noise level corresponding to about 2.6 nm. According to this crude estimate, the pick-up signal for a Stern-Gerlach test should be detectable even with room temperature copper resonator.

The sensitivity to this form of excitation is very different in a storage ring and a linac beam line. Because of the absence of stored beam, a linac-based test of polarimetry would have less sensitivity to the induced verticle motion than a storage ring test. But, in a linac, because each bunch is polarized individually, the resonance can build up for times longer than Q_rT_r, where $T_r = 1/f_r$ is the resonator period. After this time a constant maximum signal will be observable downstream. In a storage ring, the spin coherence time (SCT) is limited by polarization decay due to decoherence. This limits the ring-up time to be comparable to SCT which, if it is less than Q_rT_r, limits the polarimeter amplitude accordingly. Furthermore, once the storage ring beam is depolarized, no Stern-Gerlach signal survives at all.

(2) **Room temperature copper cavity.** The storage ring SCT limitation is unlikely to be important for room temperature copper resonator. Because of the relatively low value of Q_r, the ring-up time will be quite short. But the ring-up amplitude will be correspondingly small. In a linac, the ring-up amplitude will be correspondingly small, but the Stern-Gerlach signal will persist indefinitely, making its detection easier.

Parameters needed to compare and contrast these methods can be obtained from Ramo, Whinnery, and Van Duzer[**9**]. The surface resistance of room temperature copper is $R_s = 2.61 \times 10^{-7}/\sqrt{f_r}$ and the Q-value of our shallow resonator is given, approximately, by

$$Q_r(\text{R.T. copper}) \approx \frac{\pi}{\sqrt{2}} \frac{\eta}{R_s} \frac{b}{a} \approx \frac{\pi}{\sqrt{2}} \frac{377}{2.61 \times 10^{-7}/\sqrt{f_r}} \frac{b}{a}, \tag{6}$$

where a and b are cavity dimensions given in Figure 2(c), and $\eta = 377\,\text{ohms}$ (which is the Ramo symbol for our previously-introduced free space impedance Z_0.) At GHz frequencies the storage ring SCT can be expected to be greater than $Q_r T_r$, because of the relatively small value of Q_r, of order 10^4.

(3) **Superconducting niobium cavity.** Except for the vastly lower value of R_s, for a superconducting niobium cavity the same formulas mainly apply as have just been given for copper. But the discussion of spin coherence time in the storage ring needs to be revised. Since the superconductor value of Q_r can be greater by at least four orders of magnitude, the resonator ring-up time duration and peak amplitude will be greater by this same factor of 10^4. There is a corresponding increase in Stern-Gerlach sensitivity. This improvement factor applies in full for linac beam line polarimetry. But the improvement factor in a storage ring may not be this great, because of the SCT limitation.

(4) **Fully-instrumented, loaded Q, Stern-Gerlach cavity.** The tests listed so far have been "low tech" in that no instrumentation is required other than what is automatically present in storage ring control systems. Of course ultimate polarimetry performance will depend on extensive (and expensive) cryogenic RF design as well as sophisticated instrumentation. If and when Stern-Gerlach resonance has been unambiguously demonstrated, sufficient funding for ultimate precision should become easily justifiable. Any subsequent development would be performed at a lab such as Cornell, Jefferson Lab, COSY lab, Juelich, Germany, or ELSA lab, Bonn Germany. Significant CAD design work for a superconducting helical coil resonant polarimeter has already been performed by Evgeny Zaplatin at the COSY lab.

(5) **Proton and deuteron EDM measurement.** Another benefit of low temperature operation, as important as the increased value of Q_r, is the reduction in thermal noise. For measuring the electric dipole moments of the proton or the deuteron, the Stern-Gerlach polarimeter signal will be considerably weaker than for electrons. The magnetic dipole moments are about three orders of magnitude smaaller and the particles are barely relativistic. But, because resonant polarimetry is essential for measuring their EDMs it is important to investigate the instrumentation sensitivity necessary for hadron Stern-Gerlach

polarimetry to be useful. Certainly superconducting cavities are required, both for acceptably high Q and for acceptably low thermal noise.

2. Narrowing the options

Formal theoretical development begins with Section 3: "Waveguide mode representation by skew plane waves". The present section surveys the motivation for resonant polarimeter, and indicates some of the important issues. They include: particle type—electron or hadron; accelerator type—linac or storage ring; beam polarization—longitudinal or transverse; cavity mode–TM or TE, and so on. Once all these issues have been resolved, experimental procedures, sensitivities, and backgrounds can be addressed.

This section begins with a brief historical review of transformation properties of magnetic dipole moments. The main result of this review is to refuse to assign any intuitive physical properties to "magnetic dipole moment" in any frame other than the rest frame. Its value, μ^*, is a frame-independent physical constant. Having accepted this, it is not important to understand controversies concerning Lorentz transformation of the magnetic dipole moment, since no such transformation will figure in the remainder of the paper. This section continues its discussion of what *is not to be used,* by warning against the introduction of "magnetic potential energy" in any frame other than the particle rest frame. Stern-Gerlach interaction between cavity and particle is represented entirely by a standard 3-force. Rather than relying on "conservation of mechanical plus potential energy" one can simply evaluate the work done by the Stern-Gerlach force applied to the particle by the cavity magnetic field.

The final topic in this section is more important; it sketches the procedure that *is to be used* in the remainder of the paper for calculating Stern-Gerlach cavity excitation.

2.1. Resonant polarimetry motivation. The interest in resonant polarimetry has been driven recently by plans for measuring electric dipole moments (EDMs) of fundamental particles, especially proton, deuteron and electron. However this paper is restricted just to planning resonant polarimetry tests and not EDM experiments.

Calculations in this paper are purely classical, not quantum mechanical (other than accepting that point particles can have finite magnetic moments). Bohr and others have used the Heisenberg uncertainty principle to show that the Stern-Gerlach force cannot be used to measure the magnetic moment of a solitary electron. To circumvent this we discuss only coherent bunches of, say, 10^{10} electrons or other particles, over spin coherence times (SCT) short enough, that the magnetic moment of the bunch is (at least almost) equal to the sum of the individual magnetic moments.

Tests to demonstrate resonant polarimetry (for the first time) have been contemplated using polarized electron beams, either from a linac, such as at Jefferson Lab, or in a circular ring such as ELSA, at Bonn, Germany. There is also the possibility of using polarized proton or deuteron beams, for example at the COSY ring in Jülich, Germany.

Both transverse and longitudinal polarimetry is required for EDM measurements but, since resonant polarimetry has never been demonstrated, the immediate task is

to determine the more promising approach. I have previously[**10**][**11**] emphasized longitudinal polarimetry, using a solenoidal resonator, and some of the references remain attached to this paper. Recent thinking has been that it is preferable to use a conventional cylindrical or rectangular resonator. It is the difficulty anticipated in developing an unconventional superconducting cavity that leads to this recommendation.

To simplify the formulas, except for an appendix displaying cylindrical resonator modes, this paper is restricted to rectangular resonators. This is consistent with the conclusion already mentioned and supported later in the paper, that cylindrical resonators are unsatisfactory for Stern-Gerlach polarimetry. To lend concreteness, formulation is based initially on the configuration shown at the top left of Figure 1, superceded later by the configuration at the top right. Though the formulation here is very different, up to the point where a canted resonator is introduced, the results seem to be equivalent to those given by Conte et al., first in reference[**2**], then in later papers[**12**][**13**]. The same logic that rules out cylindrical resonators also rules out conventional cavity orientation in which beam line and cavity axis coincide. The cavity selected for the first test of Stern-Gerlach polarimetry is shown at the top right of Figure 1.

The fact that the electron's magnetic moment is three orders of magnitude greater than the proton's favors starting with electrons. Electron beam tests can either be at high, GeV-scale energies, probably using a polarized storage ring electron beam such as the ELSA ring at Bonn or CEBAF, or at low, multi-MeV energies, in a polarized electron injection line such as at Jefferson lab. The dependence on beam energy or, rather, on the relativistic γ factor has been controversial. So it is essential for this issue to be understood first.

For first demonstrating the feasibility of resonant polarimetry one wishes to identify whether longitudinal or transverse polarimetry is more promising. To understand the relative sensitivity it is important first to understand the Lorentz transformation of relevant physical parameters between the laboratory frame (in which the resonator is stationary) and the rest frame (in which the design beam particle is stationary).

Much discussion has centered on the Lorentz transformation of the "magnetic dipole moment" (MDM). The first important point to be made in this paper is that the magnetic dipole 3-vector is not, in fact, a relativistic covariant; so there is no meaningful way of "Lorentz transforming" it. Vast experience, both experimental and theoretical, has been acquired concerning MDMs in particle rest frames. But this is the only frame in which physical intuition based on this experience can be applied. There are various ways, in frames other than the rest frame, of introducing a parameter going by the name "magnetic dipole moment", but this does not permit one to extrapolate rest frame experience to moving frames, based on the "magnetic dipole moment" name. In short the physical interpretation of MDMs in moving frames needs careful treatment.

As just stated, non-relativistic behavior of the rest frame MD vector $\mathbf{m_0}$ is thoroughly understood and verified by vast experimental experience. Spin precession at relativistic energies in storage rings is also well understood. But, for calculating the excitation caused by passage of a point magnetic moment through a resonator, stationary in the laboratory, transformation between frames is necessary. Even defining

a "laboratory magnetic moment" of a moving particle is ambiguous and ill-advised. It is safer to analyse the interaction between particle and resonator in the rest frame of the particle.

2.2. Why it is wrong to Lorentz transform particle MDM's. Resonant polarimetry was first proposed in 1993 by Derbenev[**1**]. An experimental test was proposed[**3**] in 2001, but not performed. At that time the Lorentz transformation of magnetization and material magnetic dipole moments (MDMs) between coordinate frames was controversial. Some of the history is described in reference [**14**]. This has now been clarified, for example by Kholmetskii, Missevitch and Yarman[**17**]. These authors identify four physically different possible MDM definitions: "configurational", "source", "force" and "elementary particle". In the rest frame all four of these definitions are equivalent; $\mathbf{m_0}^c = \mathbf{m_0}^s = \mathbf{m_0}^f = \mathbf{m_0}^{ep}$. The Kholmetskii et al. paper concentrates on just the first three of these definitions. They defer to Bargmann, Michel and Telegdi (BMT), Jackson[**18**], Hagedorn[**19**], etc. for establishing the Lorentz transformation properies of $\mathbf{m_0}^{ep}$, which applies only to elementary point particles.

In his Section 9.6C, Hagedorn[**19**] discusses multiparticle systems in which individual particle magnetic moments and orbital magnetic moments contribute to magnetization of macroscopic media. Before addressing transformation properties of $\mathbf{m_0}^{ep}$ we briefly review the Kholmetskii paper.

The lab frame configuration[1] value $\mathbf{m}^c$, differs from the source and force values, which are equal; $\mathbf{m}^s = \mathbf{m}^f$. The "source" value $\mathbf{m}^s$ is needed to calculate the magnetic fields (due to their MDMs) of the moving charges. The force value $\mathbf{m}^f$ is needed for calculating the force on a moving magnetized medium.

For "source" and "force" definitions, the transformation derived by Kholmetskii are

$$\mathbf{m}^{s,f} = \mathbf{m_0}^{s,f} - \left(1 - \frac{1}{\gamma}\right)(\mathbf{m_0}^{s,f} \cdot \hat{\mathbf{z}})\,\hat{\mathbf{z}}. \tag{7}$$

As a result the transverse and longitudinal transformations are different;

$$\begin{aligned} \mathbf{m}_\perp^{s,f} &= \mathbf{m_0}_\perp^{s,f}, \\ \mathbf{m}_\parallel^{s,f} &= \frac{1}{\gamma}\,\mathbf{m_0}_\parallel^{s,f}. \end{aligned} \tag{8}$$

It may seem natural to presume that the transformation of spin vector from rest frame angular momentum 3-vector $\mathbf{s_R}$ to laboratory frame value $\mathbf{s_L}$ should be just like Eq. (7). But Jackson[**18**] (or alternatively Hagedorn[**19**]) show that the spin transformation corresponding to Eq. (7) should actually be a 4-vector transformation,

$$S_L = (s_{0L},\ \mathbf{s_L}) = \big(\gamma\beta(\hat{\mathbf{x}} \cdot \mathbf{s_R}),\ \ \mathbf{s_R} + (\gamma - 1)\,(\mathbf{s_R} \cdot \hat{\mathbf{z}})\,\hat{\mathbf{z}}\big). \tag{9}$$

In deriving this transformation it has been assumed that the rest frame 4-vector is $(0, \mathbf{s_R})$; i.e. the time component vanishes. To make comparison with Eq. (7) easier, we

[1]By the "configuration" definition the MDM is loop area times loop current, with current density and loop dimension transformed individually. Kholmetskii et al. explain how the laboratory frame MDM value value derived this way needs special (and quite complicated) treatment that depends on what laboratory quantity is being calculated. In this way they recover self-consistency of "c", "s", and "f" definitions.

now revert to the notation that $\mathbf{s_0}$ and $\mathbf{s}$ are, respectively, rest frame and laboratory frame spin 3-vectors. The factor multiplying $\mathbf{s}$ to produce $\mathbf{m}^{ep}$ is a measurable, frame-independent, physical constant. In this notation the transformation from $\mathbf{s_0}$ to $\mathbf{s}$ is given by

$$\mathbf{s} = \mathbf{s_0} + (\gamma - 1)\,(\mathbf{s_0} \cdot \hat{\mathbf{z}})\,\hat{\mathbf{z}}. \tag{10}$$

Because this is just a part of a 4-vector Lorentz transformation, it should not be surprising that it differs from Eq. (7). Of course Eqs. (8) also change; to

$$\begin{aligned} \mathbf{s}_\perp &= \mathbf{s_0}_\perp, \\ \mathbf{s}_\parallel &= \gamma \mathbf{s_0}_\parallel. \end{aligned} \tag{11}$$

One sees (especially for electrons) this makes a huge change compared to Eqs. (8) in the relative γ dependence of transverse and longitudinal components.

This seeming ambiguity has elicited considerable discussion for more than a decade. Here it will be shown that this whole discussion has been inappropriate. For calculating Stern-Gerlach forces only truly covariant relativistic quantities (4-scalars, 4-vectors, 4-tensors, etc.) should be transformed between frames.

2.3. Outline of the resonator excitation calculation. It has just been shown that Lorentz transformation between reference frames of the "magnetic dipole vector" $\mathbf{m}$ is ambiguous. In fact, none of the transformations exhibited so far will be used. Only the rest frame magnetic moment $\mu^*\hat{\mathbf{m}}_0$, with magnitude $|\mu^*|$, will enter subsequent formulas.

We are primarily interested in calculating the "excitation" caused by the passage of a point particle with velocity $V\hat{\mathbf{z}}$ and rest frame MDM vector $\mathbf{m}_0$ through a resonant cavity of length d, that is stationary in the laboratory. This is illustrated in Figure 3. The lower part of this figure illustrates the situation in a frame K_0 which is a particle rest frame applicable at the instant the center of the resonator passes.

To reduce ambiguity, let us specify "excitation" to mean "change in laboratory energy stored in the resonator". Calculating this energy change is analogous to the well-understood calculation of the energy deposited or extracted by a charged particle of mass m_p, charge e_p, velocity $V\hat{\mathbf{z}}$, and mechanical energy $\mathcal{E}_p = \gamma_V m_p c^2$, while passing through an RF accelerating cavity of length d, stationary in the laboratory. As viewed in the rest frame, the passing cavity length is d/γ_V and time spent inside the cavity by the particle is $(d/\gamma_V)/V$. For a particle traveling with speed V in the laboratory, the laboratory time interval dt and the "proper time" duration ds (the time measured by a clock traveling with the particle) are related by

$$ds = \frac{dt}{\gamma_V}. \tag{12}$$

If the 4-momentum of a particle is to change, it has to be because force has been applied. In the laboratory (in MKS units) the time rate of change of 3-momentum $\mathbf{p}$ caused by force 3-vector $\mathbf{f}$ is

$$\mathbf{f} = \frac{d\mathbf{p}}{dt} \quad \Big(\overset{\text{e.g.}}{=} e\mathbf{E} + e\mathbf{V} \times \mathbf{B} \Big), \tag{13}$$

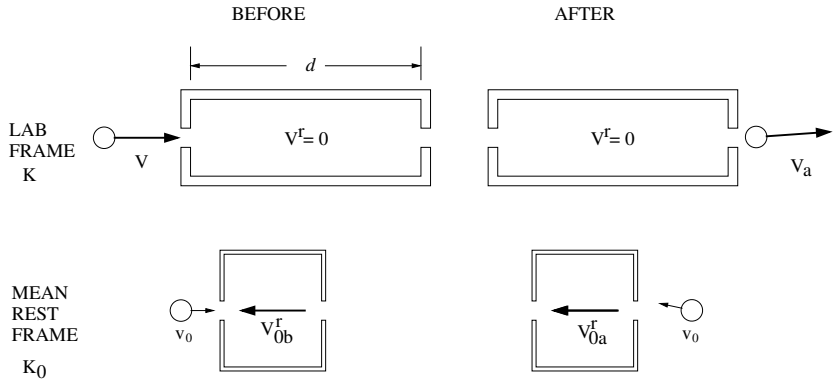

FIGURE 3. Pictorial representations of interaction between relativistic particle and resonant cavity, as viewed both from the laboratory and from a "mean rest frame" (the electron rest frame at the instant the electron passes the center of the resonator). $v_0\hat{\mathbf{z}}$ is the small, non-relativistic, particle velocity of the particle in K_0 frame. It illustrates the particle direction reversal during the passage. The resonator velocity is unchanged in the encounter; $V^r_{0a} = V^r_{0b} = -V$.

where the Lorentz force is given as an example of a relativistically-valid force definition. (Among other things, demonstration of this validity uses the fact that charge e is a true scalar invariant.) The magnetic moment μ^* will play the same roll for Stern-Gerlach excitation as does e for electromagnetic interaction.

The 4-force G is the (proper) time rate of change of 4-momentum $P = (\mathcal{E}/c, \mathbf{p})$,

$$\begin{aligned} G = \frac{dP}{ds} &= \gamma_V \left(\frac{d\mathcal{E}/c}{dt}, \frac{\mathbf{p}}{dt} \right) = (\gamma_V \mathbf{f} \cdot \mathbf{V}/c, \gamma_V \mathbf{f}) \\ &= \left(\gamma_V \beta_V f_\parallel, \gamma_V (\mathbf{f}_\parallel + \mathbf{f}_\perp) \right) \end{aligned} \tag{14}$$

where the 3-vector $\mathbf{f}$ has been decomposed into parallel and perpendicular (to $\mathbf{V}$) components. This shows that a force cannot change the energy in any frame in which the force is transverse. This is a well known property of the Lorentz force; a magnetic force does not change the particle energy.

Resonant polarimetry depends on the existence in the rest frame of a "magnetic potential energy",

$$U^m_0(t_0, \mathbf{x}_0) = -\mu^* \hat{\mathbf{m}}_0 \cdot \mathbf{B}_0(t_0, \mathbf{x}_0) \tag{15}$$

of a particle with magnetic moment $\mu^* \hat{\mathbf{m}}_0$. Unfortunately, in time-varying situations, gauge invariance can make the transformation of electromagnetic potential ambiguous. For example, in the absence of charge (as applies inside a waveguide or waveguide resonator), the electric potential Φ^e can be made to vanish identically by choosing the Coulomb gauge.

(Incidentally, this *does not* contradict the observational fact that a waveguide resonator can be used to accelerate particles, as one might be tempted to conclude based on a supposed, frame-independent, "conservation law for potential energy" $e\Phi^e$. Consistent with such a law would be the requirement that energy change $e\Delta\Phi^e$ necessarily

vanishes in passing from well before, to well after, an isolated RF cavity. The existence of such a "law" for electric charge RF acceleration would contradict the existence of RF accelerators.)

Hagedorn[**19**], Eq. (9.32), shows that the rest frame angle θ_R between the velocity and the spin vector direction is constant for boosts parallel to the magnetic field, This makes it possible to analyse independently the Stern-Gerlach influences of transverse and longitudinal beam magnetization.

It is convenient to formulate the calculation with an (abundantly valid) impulsive approximation, in which the integrated Stern-Gerlach momentum imparted to a particle passing through the resonator is small enough to justify neglecting its displacement during the encounter. One also notes that it is only the longitudinal component of force that can change the energy of a particle.

The laboratory frame transverse electric and magnetic fields $\mathbf{E}(x,t)$ and $\mathbf{B}(x,t)$ in various resonant cavities, as functions of position x and time t, are given later. For now we assume these fields are known. For our geometry, with rest frame advancing along the positive z axis, Jackson's Eq. (11.149) (switched to SI units) gives formulas for the transformation from transverse laboratory electric and magnetic fields $E_y\hat{\mathbf{y}}$ and $B_x\hat{\mathbf{x}}$ to rest frame fields $E_{0y}\hat{\mathbf{y}}$ and $B_{0x}\hat{\mathbf{x}}$;

$$\begin{aligned}\mathbf{E}_0 &= \gamma_{_V}(E_y\hat{\mathbf{y}} + \beta_{_V}\hat{\mathbf{z}}\times cB_x\hat{\mathbf{x}}) = \gamma_{_V}(E_y + \beta_{_V}cB_x)\,\hat{\mathbf{y}}\\ \mathbf{B}_0 &= \gamma_{_V}(B_x\hat{\mathbf{x}} - \beta_{_V}\hat{\mathbf{z}}\times E_y\hat{\mathbf{y}}/c) = \gamma_{_V}(B_x + \beta_{_V}E_y/c)\,\hat{\mathbf{x}}.\end{aligned} \tag{16}$$

These formulas assume that the electric field is aligned with the y-axis, and the magnetic field with the x-axis. Transverse electric and magnetic waveguide fields are always orthogonal, deviating from these formulas only by an azimuthal rotation of these fields around the z-axis. In this sense Eqs. (16) are sufficiently general. We have specialized in this way so that subsequent formulas can avoid vector operator notation.

3. Waveguide mode representation by skew plane waves

3.1. Skew plane waves. I have developed a special formalism for treating the effect of Stern-Gerlach forces acting on a particle with magnetic dipole moment $\mathbf{m}$ passing through a resonant cavity. The procedure is based on superpositions of skew plane wave pairs, where a skew plane wave is introduced first. The idea for this represention was obtained from the book, *The Plane Wave Spectrum Representation of Electromagnetic Fields,* by P.C. Clemmons[**20**].

There are a few justifications for introducing an unconventional waveguide mode formalism. For the low order, rectangular waveguide modes favored for Stern-Gerlach cavity resonance, a total of four skew waves is sufficient to represent the cavity fields. Rather than interacting with a formally complicated resonator mode, the beam can be visualized as interacting with just four plane waves having coplanar wave vectors, with the beam orbit itself lying in the common plane. Later, when a canted resonator is introduced, since each of the four waves is already slanted relative to the beam path, the effect of a slant of the beam path itself does not greatly complicate the picture.

As well as reducing the complexity of the formulas this makes it natural to represent the Stern-Gerlach force as a superposition of just four forces. This purges any temptation to introduce a "magnetic potential energy" in any frame other than the electron rest frame. There is a further minor benefit for deriving results by an independent formalism; formulas can be checked against results obtained by a different approach. There is no reason to doubt that the skew wave formalism is equivalent to standard waveguide formalism.

A "skew wave" of frequency ω, as here defined, is a plane wave propagating in the direction of unit vector $\mathbf{n}$, as shown in Figure 4. Its angle relative to the z-axis is α and its eventual purpose is to be combined with other skew waves to produce a waveguide mode, either TE or TM, propagating along the z-axis. As drawn in the figure, because the electric field has no z-component, waves of this type can be used to produce TE modes. Using notation copied from Clemmons, the vectors in the figure,

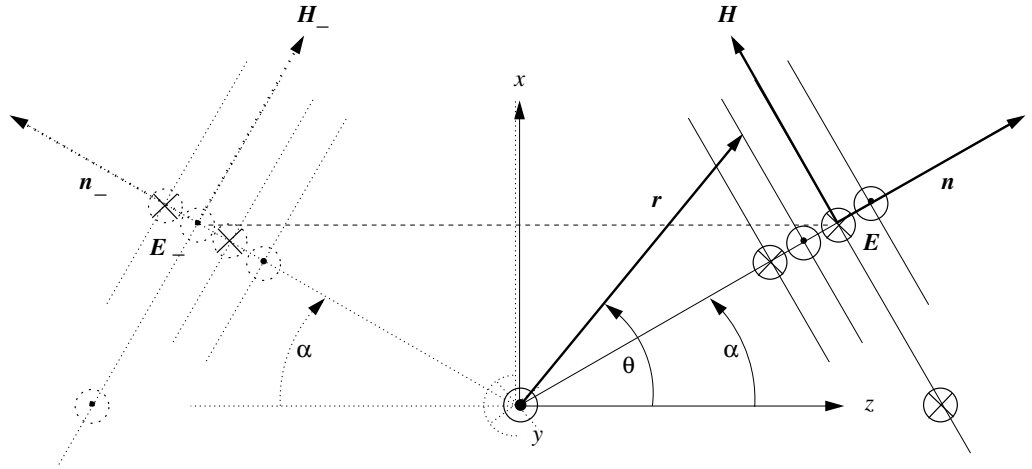

FIGURE 4. Skew wave component for TE modes advancing toward more positive z. Initially the faint figure on the left is to be ignored. It represents a backward-travelling skew wave to be superimposed later to match the electric and magnetic boundary conditions on the $z = 0$ plane.

are represented, for TE modes, by

$$\mathbf{n} = (\sin\alpha, 0, \cos\alpha), \tag{17}$$

$$\mathbf{r} = (r\sin\theta, r_y, r\cos\theta), \tag{18}$$

$$\mathbf{n}\cdot\mathbf{r} = r(\sin\alpha\sin\theta + \cos\alpha\cos\theta) = r\cos(\theta-\alpha), \tag{19}$$

$$\mathbf{E} = (0, -1, 0)\, e^{-jkr\cos(\theta-\alpha)}\, E, \tag{20}$$

$$\mathbf{H} = (\cos\alpha, 0, -\sin\alpha)\, e^{-jkr\cos(\theta-\alpha)}\, \tilde{E}, \tag{21}$$

where $k = 2\imath/\lambda$ and $\omega/k = c$. The electric field amplitude of this wave is E. Eq. (21) employs an unconventional treatment of units that is flagged by the presence of the overhead tilde in symbol $\tilde{E}$. The tilde is to be taken to mean that "the units will be sorted out later". Appearing in Eq. (20), E has the electric field units matching $\mathbf{E}$.

But Eq. (21), seemingly "equating" a magnetic to an electric field, looks dimensionally inconsistent, at least in MKS units. The essence of these two equations is that, for free space EM plane waves, in the most convenient units, the magnetic and electric field amplitudes would be the same. As written, the choice of consistent units can be deferred. For these two equations to actually be dimensionally consistent in MKS units, $\tilde{E}$ would would have to be replaced by E/η in Eq. (21), where η is the "free space impedance" of 377 Ohms.

A time variation $\exp j\omega t$ factor multiplying all fields has also been suppressed. The wave number k is given by

$$k = \omega\sqrt{\epsilon_0\mu_0}. \tag{22}$$

For $0 < \alpha < \pi/2$ this wave is advancing toward more positive z. The skew wave phase is definced by

$$\phi_\alpha(t, \mathbf{r}) = \omega t - \mathbf{k}\cdot\mathbf{r} = \omega t - kr(\sin\alpha\sin\theta + \cos\alpha\cos\theta). \tag{23}$$

where $\mathbf{k} = k\mathbf{n}$. As such, for fixed α, the wave phase ϕ_α is defined throughout space-time.

Usually what will be most relevant is the skew wave phase at the space-time location of a particle moving with speed V, so that $r = Vt$, along a line passing through the origin at angle θ. The "proper phase" is the wave phase advance at the space-time position of the particle. So $\phi_\alpha(t, 0) = \omega t$ is the phase of a wave, measured at the location of a particle at rest at the origin in the laboratory. For a particle at longitudinal position $z = r\cos\theta$, moving from the space-time origin at angle θ, the proper phase is

$$\Delta\phi_{\alpha,\theta}(z) = \frac{kz}{\cos\theta}\left(\frac{1}{\beta_{_V}} - \cos(\alpha - \theta)\right). \tag{24}$$

The Δ is included in the $\Delta\phi_{\alpha,\theta}$ symbol to indicate that it represents the proper phase, assuming the phase at the origin is zero.

An important property of wave phase is that it has the same value in different reference frames. However it is only the $\phi_{\alpha,\theta}$ proper phase for which this property is easily applied. Using this invariance, when evaluated in its own rest frame, the value of wave phase at a particle's position in space-time is given by $\phi_{\alpha,\theta} = \omega_0 t_0$, where subscript "0" indicates coordinates in the particle rest frame. This justifies referring also to $\phi_{\alpha,\theta}$ as a proper phase, or "proper phase interval", because the phase at the space-time origin is assumed to be zero in all reference frames. For a particle traveling at angle θ in the laboratory, when the longitudinal position is $z = d$, for example at the exit of a cavity of length d, the proper phase is obtained by substituting $z = d$ in Eq. (24).

When needed, TM modes can be constructed from skew waves of the form

$$\mathbf{E} = (\cos\alpha, 0, -\sin\alpha)\, e^{-jkr\cos(\theta-\alpha)}\, E, \tag{25}$$

$$\mathbf{H} = (0, 1, 0)\, e^{-jkr\cos(\theta-\alpha)}\tilde{E}. \tag{26}$$

3.2. Skew plane wave pairs, pairs of pairs, etc. A possible skew wave to complement the TE wave just introduced, is symmetrically on the other side of the z axis, advancing into the positive z hemispace, as shown in Figure 5. Such a pair

of waves can be used to match a boundary condition along a (perfectly conductive) side wall of a rectangular waveguide. This wall could, for example, be in the (y, z) plane along the z-axis. This would not be acceptable if, as we assume, there is a beam traveling along the z-axis. But conductive walls can be situated along other lines parallel to the (y, z) plane, but displaced from, the z-axis.

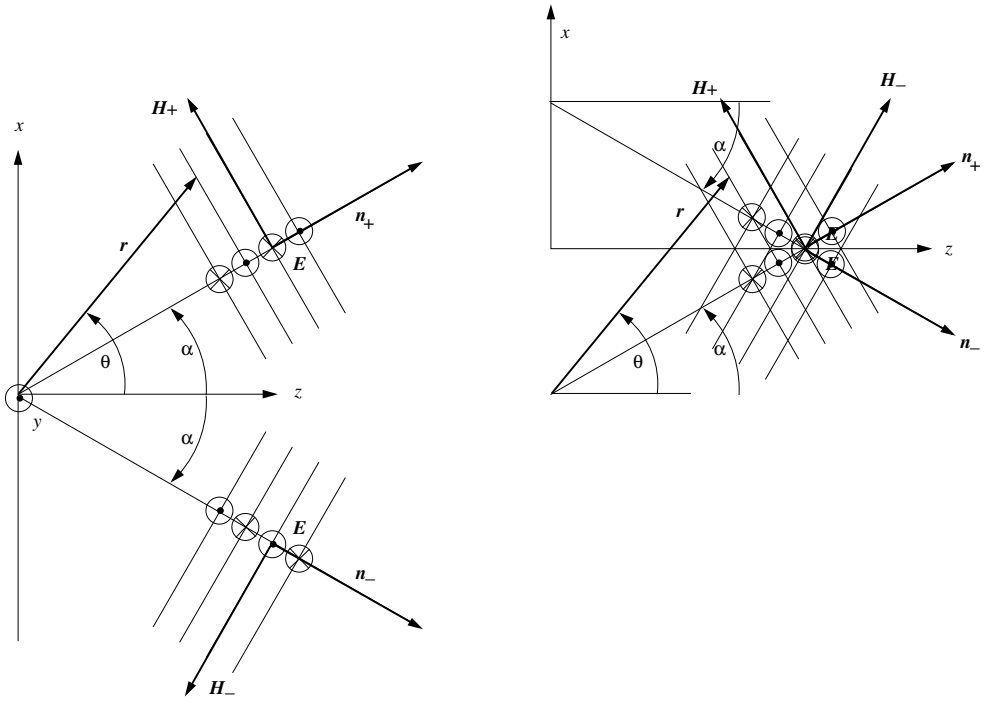

FIGURE 5. On the left, a pair of TE skew waves advancing toward more positive z. On the right, the same two waves but at a point where on-axis electric vectors interfere constructively. These skew waves are to be used later to produce resonator modes favorable for resonant polarimetry.

Vectors for the two waves are

$$\mathbf{n}_\pm = (\pm \sin\alpha, 0, \cos\alpha), \tag{27}$$

$$\mathbf{r} = (r\sin\theta, r_y, r\cos\theta), \tag{28}$$

$$\mathbf{n}_\pm \cdot \mathbf{r} = r\cos(\theta \mp \alpha), \tag{29}$$

$$\mathbf{E}_\pm = (0, \mp 1, 0)\, e^{-jkr\cos(\theta\mp\alpha)}\, E_\pm, \tag{30}$$

$$\mathbf{H}_\pm = (\pm\cos\alpha, 0, -\sin\alpha)\, e^{-jkr\cos(\theta\mp\alpha)}\, \tilde{E}_\pm. \tag{31}$$

These two waves can either be added, $\mathbf{H}_+ + \mathbf{H}_-$ or subtracted, $\mathbf{H}_+ - \mathbf{H}_-$, with corresponding expressions for $\mathbf{E}$. Another possible superposition results by shifting the phase of one wave relative to the other, as in $\mathbf{H}_+ \pm i\mathbf{H}_-$. But one does not have complete freedom in superimposing these fields though; in a waveguide, it is reflections from the waveguide walls, as imposed by boundary conditions there, that make the waves identical to what they would be in free space.

Other skew wave pairs can be formed by azimuthal rotation around the z-axis. Rotation by $\pi/2$ is equivalent to replacements $x \to y, y \to -x$. Further superpositions are also possible, either discrete, such as those already mentioned, or continuous, formed by superimposing continuous azimuthal distributions. The former are appropriate for rectangular wave guides. The latter can, presumebly, be superimposed to construct cylindrical waveguide modes, with their Bessel function radial dependencies. Only discrete cases will be attempted here.

Propagating waveguide fields can be visualized as plane waves being reflected from the walls of the waveguide. With discrete superpositions it is possible to represent forward propagation in rectangular waveguides. In general this will require at least two pairs of skew waves, one representing horizontal reflections, the other vertical. For circular waveguides continuous superpositions are required.

To represent resonant cavity oscillations it is necessary to employ backward traveling waves. The backward waves can be visualized as being reflected by entrance and exit, transverse, conductive planes. For a rectangular guide this will double the typical number of skew wave pairs required, for example from four to eight. Backward waves are easy enough to visualize but, when Lorentz transforming along the z axis, it is necessary to treat forward and backward waves separately.

To keep the formulas simple we will concentrate first on a single skew wave, finding the momentum impulse it imparts to a passing magnetic moment. Restricting the discussion to discrete superpositions, means we are assuming rectangular waveguides and resonators, even though circular resonators may be used in practice. Physical intuition suggests that behaviors of circular and rectangular guides will not differ significantly. It is only the introduction of a canted resonator that favors rectangular over circular resonators.

With superposition applicable, the impulses from all skew waves simply have to be added. If all contributions were constructive the total momentum impulse would be roughly equal to the impulse from one field multiplied by the number of fields. But, of course, destructive interference has to be anticipated in some cases. Destructive interference of forward and backward wave amplitudes at input and output surfaces is what allows the boundary conditions there to be met. The eventual summing of the momentum impulses from the individual skew wavess making up a given mode will have to account for these coherent interferences.

3.3. Lorentz transformation of skew waves. Our skew wave fields propagate at angle α relative to the z axis in the lab frame. We need to boost them along the z axis, from the laboratory to the rest frame. A standing wave in the resonator is made up of a superposition of forward/backward pairs. Though the forward and backward propagation angles relative to the z-axis are the same in the laboratory, these angles will be different in the particle rest frame. Lorentz transformation is therefore required from unprimed laboratory frame coordinates, to subscript "0" variables in a frame moving with velocity V along the positive z-axis in the laboratory.

In his Section (11.3-D), *Relativistic Doppler Shift,* Jackson develops the formulas we need. The wave 4-vectors for forward and backward waves in the lab and rest frames are $K_\pm = k(1, \sin\alpha, 0, \pm\cos\alpha)$ and $K_0 = k_{0\pm}(1, \sin\alpha_{0\pm}, 0, \cos\alpha_{0\pm})$. (Here I have

introduced a special (large font) symbol α to represent an angle guaranteed to be in the range $0 \leq \alpha < \pi/2$.) These transform as true 4-vectors. For forward and backward skew waves in the laboratory indicated by "±" subscripts, $\sin\alpha_+ = \sin\alpha_- \equiv \sin\alpha$ and $\cos\alpha_\pm = \pm\cos\alpha$. With $\omega = kc$, the Lorentz transformations are

$$\omega_{0\pm} = \gamma_V \omega(1 - \beta_V \cos\alpha_\pm), \tag{32}$$

$$\tan\alpha_{0\pm} = \frac{\sin\alpha}{\gamma_V(\pm\cos\alpha - \beta_V)}, \tag{33}$$

where α is required to be in the range $0 \leq \alpha < \pi/2$. For example, $\alpha = 60°$, $\sin\alpha_- = \sin\alpha_+ = \sin\alpha = 0.866$, $\cos\alpha_+ = \cos\alpha = 0.5$, $\cos\alpha_- = -0.5$.

Notice, in the fully-relativistic regime where $\beta_V \approx 1$ and $\gamma_V >> 1$, that

$$\tan\alpha_{0\pm} \approx -\frac{\sin\alpha}{1 \mp \cos\alpha}\frac{1}{\gamma_V} \quad \text{implies} \quad \alpha_{0\pm} \approx \pi - \tilde{\alpha}_{0\pm}, \tag{34}$$

where we have introduced a "small" angle $\tilde{\alpha}_{0\pm}$ for which $0 < \tilde{\alpha}_{0\pm}, << \pi/2$. That is, in the rest frame, not only are both waves "backward", the backward wave deviates only by the small $\tilde{\alpha}_{0\pm}$ angle from the negative z-axis, and even more so with increasing γ_V.

Over most of the possible angular range for α, the same approximation will be valid, especially as γ_V becomes larger and larger. For example, suppose α is changed to $\alpha + \Theta$, where $\Theta = 30°$; that is, $\alpha = 90°$, $\sin\alpha = 1$, $\cos\alpha = 0$, then $\alpha_0 \approx \pi - 1/\gamma_V$. Or suppose α is changed to $\alpha - \Theta$; that is, $\alpha = 30°$, $\sin\alpha = 0.5$, $\cos\alpha = 0.866$, then $\alpha_0 \approx \pi - 3.73/\gamma_V$. For this numerology to be typical, $\alpha + \Theta$ should not exceed 90° and $\alpha - \Theta$ should remain greater than zero. All these approximations are quite good, provided γ_V is greater than, say, 30.

Under these conditions it will be legitimate to use the approximation

$$\tilde{\alpha}_{0\pm} = \pi - \alpha_{0\pm} \approx \frac{\sin\alpha}{1 \mp \cos\alpha}\frac{1}{\gamma_V}, \tag{35}$$

Later it will prove advantageous to measure α relative to an axis displaced by a positive angle Θ that can be positive, in which case the rest frame angles will be referred to as $\alpha_{0\pm}$. In this case approximation (35) becomes

$$\tilde{\alpha}'_{0\pm} = \pi - \alpha'_{0\pm} \approx \frac{\sin(\alpha_\pm - \Theta)}{1 \mp \cos(\alpha_\pm - \Theta)}\frac{1}{\gamma_V}. \tag{36}$$

The signs of both numerator and denominator remain unambiguous. When this approximation is valid, the following small angle approximations will also be valid;

$$\sin\alpha'_{0\pm} \approx \tilde{\alpha}'_{0\pm},\ \cos\alpha'_{0\pm} \approx 1 - (\tilde{\alpha}'_{0\pm})^2/2, \quad \text{and} \quad \tan\alpha'_{0\pm} \approx -\tilde{\alpha}'_{0\pm}. \tag{37}$$

Greatly simplifying the task is the phase transformation

$$\phi_\pm = \omega_\pm t - \mathbf{k}_\pm \cdot \mathbf{r} = \omega_{0\pm} t_0 - \mathbf{k}_{0\pm} \cdot \mathbf{r}_0, \tag{38}$$

which is the invariant scalar products of two 4-vectors. This invariance can be understood to mean that the individual phases as well as being Lorentz invariant, are equal. This is helpful in visualizing standing waves in different reference frames. Though the

frequencies and wavelengths of the two traveling waves differ, the locations of standing wave features, such as nodes or maxima, stay matched to the same points, during Lorentz transformation between frames.

For TE modes, since $\boldsymbol{\beta}_{\mathbf{V}} \cdot \mathbf{E} = 0$, Jackson's Eqs. (11.149) reduce to

$$\begin{aligned}\mathbf{E}_0 &= \gamma_V(\mathbf{E} + \boldsymbol{\beta}_V \times \mathbf{B}c),\\ \mathbf{B}_0 &= \gamma_V(\mathbf{B} - \boldsymbol{\beta}_V \times \mathbf{E}/c) + (1-\gamma_V)\,(\hat{\boldsymbol{\beta}}_V \cdot \mathbf{B})\,\hat{\boldsymbol{\beta}}.\end{aligned} \tag{39}$$

For our TE mode skew wave, the rest frame fields are

$$\mathbf{E}_0 = \gamma_V(1 - \beta_V \cos\alpha)\mathbf{E}, \tag{40}$$

$$\mathbf{B}_0 = \gamma_V(\cos\alpha - \beta_V)B\hat{\mathbf{x}} - \sin\alpha B\hat{\mathbf{z}}. \tag{41}$$

Factors such as $1-\beta_V\cos\alpha$ or $\cos\alpha - \beta_V$ might, in some contexts, be made frightening by their possible near cancellation to zero. This is never a problem in our case, even for large γ_V, with $\beta_V \approx 1$. In our case, since α is never excessively close to zero, $\cos\alpha$ is never excessively close to 1, so these factors are never excessively close to zero.

Rather than using Eq. (41) to transform the magnetic field, since we are discussing a single plane wave in both frames, the electric and magnetic field magnitudes are constrained. From Eq. (40) we also have

$$\begin{aligned}E_0 &= \gamma_V(1 - \beta_V\cos\alpha)E,\\ B_0 &= \gamma_V(1 - \beta_V\cos\alpha)B.\end{aligned} \tag{42}$$

3.4. Forward/backward wave pairs. Of the required skew wave partners needed to construct a given TE mode, the most important is the (unique) backward skew wave needed to match the conductive wall boundary condition at the entrance and exit faces of the cavity. The combined forward-backward pair produces a cavity standing wave. The laboratory length d of the cavity is equal to an integer number of laboratory half-wavelengths of the waves. The full cavity response for any particular TE mode is obtained by summing the appropriate forward/backward pairs. Other than the (quite likely) possibility of exact cancellation due to symmetry, the order of magnitude of the coherent sum can be estimated to be given by the effect of a single forward/backward skew wave pair, multiplied by the number of such pairs making up the mode.

One has to be careful to avoid possible incorrect assumptions that have not been considered so far. The standing waves in a resonant cavity are formed from forward/backward pairs. Taking $\alpha^F < \pi/2$ as the angle of the forward wave in the laboratory, then $\alpha^B = \pi - \alpha^F$ is the angle of the backward wave; it lies in the angular range $\pi/2 < \alpha^B < \pi$ in the laboratory. One possible faulty assumption is that the wave propagation angle α^F is more or less arbitrary and can, perhaps, be a "small" angle. In fact, for waves in a waveguide, α is a function of the frequency f. A typical value for the angle α can be obtained from a typical value for the phase velocity, according to the formula

$$v_p = \frac{\pm c}{\sqrt{1 - f_c^2/f^2}} = \frac{\pm c}{\cos\alpha} \overset{\text{e.g.}}{=} 2c, \tag{43}$$

where a sample numerical value is given. Here the $\pm$ option allows for the wave propagation to be either forward or backward, assuming the angle α is always measured

from the positive z-axis. Assuming forward propagation, $\cos\alpha = 0.5$. So, at least not far above waveguide cut-off frequency (which will be required for experimental reasons) α^F will actually be a "not-small" angle. From Eq. (43) one also obtains

$$\cos\alpha = \pm\sqrt{1 - f_c^2/f^2}, \quad \text{and} \quad \sin\alpha = f_c/f. \tag{44}$$

For frequencies only slightly above the cut-off frequency one can introduce a frequency difference $\Delta f = f - f_c$, with $\Delta f > 0$ being required. There is no urgent reason for approximating these relations but, for frequencies just above cut-off,

$$\sin\alpha \approx 1 - \Delta f/f_c, \quad \text{and} \quad \cos\alpha \approx \pm\sqrt{2\Delta f/f_c}. \tag{45}$$

When contemplating a wave pair that is forward/backward in the laboratory, one is tempted to visualize the pair as also being forward/backward in the rest frame. This assumption can be tested by referring to Eq. (33) and, in particular, the denominator factor $\pm\cos\alpha - \beta_{_V}$. When evaluated for the backward wave the factor $\pm\cos\alpha^B - \beta_{_V}$ is certainly negative, since both terms are negative. For α^F, this denominator factor changes sign at an angle $\overline{\alpha}$ given by

$$\overline{\alpha} = \cos^{-1}\beta_{_V} \;\overset{?}{\approx}\; \cos^{-1}\left(1 - \frac{1}{2\gamma^2}\right) \;\overset{?}{\approx}\; \frac{1}{\gamma}. \tag{46}$$

The approximations here have been marked as questionable, since they assume fully-relativistic conditions $\gamma >> 1$.

From what has been said, in the fully-relativistic regime, for resonator frequencies low enough (relative to cut-off) to be practical, α^F (because it is "not small") will certainly exceed $\overline{\alpha}$ so, again, the denominator in Eq. (33) is negative. The conclusion, for large $\gamma_{_V}$, is that skew waves forward in the lab will be backward in the rest frame; contrary to casual expectation, both backward and forward waves in the lab are backward in the rest frame.

The parameters for frozen spin electrons and protons are very different. For protons a quite low value $\gamma_{_V} = 1.25$ applies, with the result that forward and backward waves in the laboratory are also forward and backward in the rest frame. But for electrons, because they are fully relativistic, $\gamma_{_V} = 30$, both waves are backward in the rest frame. It seems safe to assume that frozen spin electron beams can be treated as ultra-relativistic, while frozen spin proton of deuteron beams have to be treated as only weakly-relativistic.

Over a full skew wave cycle the impulse imparted to the particle by the Stern-Gerlach force cancels exactly. Half-cycles are the largest wave phase interval for which the sign of the force does not change. This is the maximum impulse that can be imparted in a single passage through the cavity. The shortest effective resonator length has longitudinal phase advance equal to π. Odd-integer multiples of that length could be just as effective.

3.5. Force applied to magnetic moment. Resonant polarimetry depends on the existence, in the rest frame, of a "magnetic potential energy",

$$U_0^m(t_0, \mathbf{x}_0) = -\mu^* \hat{\mathbf{m}}_0 \cdot \mathbf{B}_0(t_0, \mathbf{x}_0), \tag{47}$$

of a particle with magnetic moment $\mu^*\hat{\mathbf{m}}_0$ in magnetic field $\mathbf{B}_0$. Following Conte et al.[**2**], *to emphasize its relativistic invariance*, the symbol μ^* stands for the signed-magnitude of the rest frame magnetic moment. Magnetic energy resembles electrical potential energy. We know though, that gauge invariance can alter the physical interpretation of electric potential energy in time-varying situations. For example, in the absence of charge (as applies inside a waveguide or waveguide resonator), the electric potential Φ^e can even be made to vanish identically by choosing the Coulomb gauge. This makes it invalid to argue that, because a particle passes from zero potential energy before a cavity to zero potential energy after a cavity, that a particle cannot be accelerated by an RF cavity. Any similar mis-application of conservation of magnetic energy has to be avoided. In this paper I refuse to introduce a magnetic energy in any frame other than the particle rest frame.

Like electric potential energy, magnetic energy $U_0^m = -\mu^*\hat{\mathbf{m}}_0 \cdot \mathbf{B}_0$ is certainly not a relativistic invariant. $\mu^*\hat{\mathbf{m}}_0$ is just the rest frame spatial part of a true 4-vector M, and the individual components of $\mathbf{B}_0$ are components of the electromagnetic tensor $F^{\mu\nu}$, which is a true 4-tensor. It seems to be impossible to construct a non-vanishing, true scalar invariant from M and $F^{\mu\nu}$, even for Lorentz transformations specialized to be boosts parallel to a single axis.

Another important difference between electric and magnetic potential energy is the dependence of U_0^m on the direction of the magnetic moment vector $\hat{\mathbf{m}}_0$. This dependence makes it appropriate to discuss separately the longitudinal $\mu^*\hat{\mathbf{z}}$ and transverse $\mu^*\hat{\mathbf{m}}_\perp$ cases. Hagedorn[**19**], Eq. (9.32), shows that the rest frame angle θ_R between the velocity and the spin vector direction is constant for boosts preserving the particle direction. This makes it possible to analyse independently the Stern-Gerlach influences of transverse and longitudinal beam magnetization.

For these reasons, rather than trying to assign meaning to magnetic potential energy in frames other than the rest frame, we will first infer the rest frame force by spatial differentiation of rest frame potential energy U_0^m. Integrating the rest frame equation of motion will then produce a rest frame 4-momentum change caused by passage of the magnetic moment through a resonator. Lorentz transformation will then produce the particle's laboratory energy change $\Delta\mathcal{E}$. The required change in resonator energy is then $-\Delta\mathcal{E}$.

It is only the longitudinal component of force that can change the energy of a particle. A sufficiently large, accumulated transverse force, in what was initially the rest frame, could cause the particle's transverse momentum to deviate significantly from zero, which could also produce a noticeable energy change in the laboratory. Neglect of any such contribution is justified by the extreme weakness of the Stern-Gerlach force.

The motivation for establishing the skew wave decomposition has been to avoid introducing "magnetic potential energy" in any frame other than the rest frame, where it is given by Eq. (47). The Stern-Gerlach force is given in the rest frame by

$$\mathbf{R}_0^m = -\mu^*\nabla\big(\hat{\mathbf{m}}_0 \cdot \mathbf{B}_0\big). \tag{48}$$

We will treat separately longitudinal magnetic moment $\mu^*\hat{\mathbf{z}}$ and transverse magnetic moment $\mu^*\hat{\mathbf{m}}_\perp$. Furthermore, concentrating just on resonator energy excitation, we

will limit the discussion to the longitudinal force components;

$$\mathbf{R}_{0z}^{mTE\perp} = -\mu^* \frac{\partial(\hat{\mathbf{m}}_{0\perp} \cdot \mathbf{B}_{0\perp})}{\partial z_0}, \quad R_{0z}^{mTE\parallel} = -\mu^* \frac{\partial(\hat{m}_{0\parallel} B_{0\parallel})}{\partial z_0}, \tag{49}$$

(The "m" superscript stands for "magnetic" force, as contrasted with, shortly to be introduced, "e" superscript standing for "electric".) Initially we are concerned only with particle motion along the z-axis, where $\theta = 0$ and $r = z$. From Eqs. (20) and (21), using $r_0 \cos(\theta_0 - \alpha_0) = z_0 \cos\alpha_0 + y_0 \sin\alpha_0$, the non-zero, on-axis, field components and dot products, and derivatives of dot products, for a single skew wave, are given by

$$E_{0y} = -e^{-jk_0 z_0 \cos\alpha_0}\, e^{j\omega_0 t_0}\, E_0, \tag{50}$$

$$B_{0x} = \cos\alpha_0\, e^{-jk_0 z_0 \cos\alpha_0}\, e^{j\omega_0 t_0}\, \tilde{E}_0, \tag{51}$$

$$B_{0z} = -\sin\alpha_0\, e^{-jk_0 z_0 \cos\alpha_0}\, e^{j\omega_0 t_0}\, \tilde{E}_0. \tag{52}$$

$$\hat{m}_{0\parallel} B_{0\parallel} = -\sin\alpha_0\, e^{-jk_0 z_0 \cos\alpha_0}\, e^{j\omega_0 t_0}\, \tilde{E}_0,$$

$$\hat{\mathbf{m}}_{0\perp} \cdot \mathbf{B}_{0\perp} = \cos\alpha_0\, e^{-jk_0 z_0 \cos\alpha_0}\, e^{j\omega_0 t_0}\, \tilde{E}_0,$$

$$(\partial/\partial z_0)\, \hat{m}_{0\parallel} B_{0\parallel} = jk_0 \sin\alpha_0 \cos\alpha_0\, e^{-jk_0 z_0 \cos\alpha_0}\, e^{j\omega_0 t_0}\, \tilde{E}_0.$$

$$(\partial/\partial z_0)\, \hat{\mathbf{m}}_{0\perp} \cdot \mathbf{B}_{0\perp} = -jk_0 \cos^2\alpha_0\, e^{-jk_0 z_0 \cos\alpha_0}\, e^{j\omega_0 t_0}\, \tilde{E}_0,$$

where the time factor $\exp j\omega_0 t_0$ has been restored, and all quantities are now being evaluated in the rest frame. Because of the multiplicity of possible wave-pair combinations, the $\pm$ designations in previous equations are confusing and have been removed. With all fields now regarded as applicable in the rest frame, all parameters and coordinates have acquired "0" subscripts.

Note that, if the laboratory frame frequency ω is regarded as fixed then, like the rest frame angle α_0 and amplitude B_0, the rest frame frequency ω_0 depends on the laboratory angle α. These quantities are related by Doppler effect formulas.

Though off-axis field dependence has been suppressed, the dependence on z_0 has been retained. In this form the fields can still be used to calculate on-axis Coulomb and Lorentz forces acting on the particle charge, as well as longitudinal Stern-Gerlach forces. But all off-axis field dependence has been suppressed by setting $\theta = 0$, and transverse Stern-Gerlach forces have been dropped.

Because the z_0 dependence is explicit, longitudinal Stern-Gerlach forces can now be calculated by differentiation, for both longitudinal and transverse beam polarization, using Eqs. (49). The fields and forces at the $z_0 = 0$ origin are then

$$E_{0y}(t_0, 0) = -e^{j\omega_0 t_0}\, E_0, \tag{53}$$

$$B_{0x}(t_0, 0) = \cos\alpha_0\, e^{j\omega_0 t_0}\, B_0, \tag{54}$$

$$B_{0z}(t_0, 0) = -\sin\alpha_0\, e^{j\omega_0 t_0}\, B_0, \tag{55}$$

$$R_{0z}^{m_\parallel TE}(t_0, 0) = -j(\mu^* B_0) \sin\alpha_0 \cos\alpha_0\, e^{j\omega_0 t_0} \omega_0/c, \tag{56}$$

$$R_{0z}^{m_\perp TE}(t_0, 0) = j(\mu^* B_0)\, \cos^2\alpha_0\, e^{j\omega_0 t_0} \omega_0/c. \tag{57}$$

Since we only need the time dependence at the rest frame origin, we have set $z_0 = 0$ in these equations. Also $k_0 = \omega_0/c$, and manifest dimensional consistency has been

restored by replacing $\tilde{E}_0$ by B_0, which is the free space plane wave magnetic field corresponding to E_0. (In MKS units $B_0 = E_0/c$.)

For future reference we note, in passing, that the longitudinal force on a charge e in a corresponding TM skew field would be given by

$$F_{0\|}^{eTM}(t_0, 0) = -eE_{0\|}\, e^{j\omega_0 t_0}, \tag{58}$$

and also that the rest frame TE forces on the MDM $\mathbf{m}$ and the rest frame TM forces on electric charge e are in the following ratios:

$$\begin{aligned} F_{0\|}^{eTM} &: R_{0z}^{m_\| TE} : R_{0z}^{m_\perp TE} \\ &= -eE_{0\|} : -jk_0(\mu^* B_0)\sin\alpha_0\cos\alpha_0 : jk_0(\mu^* B_0)\,\cos^2\alpha_0. \end{aligned} \tag{59}$$

Being in the particle rest frame, these can be regarded as exact relations, valid both relativistically or non-relativistically.

The longitudinal Stern-Gerlach force has now been put on the same footing as conventional electromagnetic forces. There is no longer any need for magnetic potential energy. This has achieved the main purpose for introducing skew waves. If one wishes, one can continue to think of the factor $\mu^* B_0$ as a magnetic potential energy, but this carries no implication that its conservation is guaranteed by any conservation law.[2]

The time dependences of the fields have now been reduced to the fields acting on a polarized particle situated at the origin in the rest frame. As mentioned previously, when the field amplitudes of other skew waves are added, the signs have to match the particular waveguide mode being represented to produce the correct coherent sum for that mode.

A single skew wave field, purely sinusoidal for all time, cannot cause an accumulating influence on a particle. But, with a resonant cavity present, the fields interior to the cavity are identical to the free space waves just calculated. For example, the backward wave reflected from the conductive exit surface of the resonator interferes with the forward wave to produce a standing wave in the cavity.

A particle is within the cavity for only a brief time interval, which limits the time during which the force is effective. The arrival time of the particle at the cavity is under external control. The essential requirement for resonant polarimetry will be to cause the particle always to arrive and leave the cavity at phases optimal for extraction of energy from the cavity to the particle or from the particle to the cavity.

We can calculate the maximum possible momentum impulse that can be administered to the particle by a skew wave during one half cycle (which is the maximum

[2]The comment concerning the effect of a possible magnetic potential energy conservation law is made only for reference in later discussion of the Conte et al. resonator excitation formalism. The issue then will be the influence of resonator end "fringe fields". In particular there is the possibility of exact cancellation in the fringe field regions of the excitation caused by forces in the interior of the cavity. If the Stern-Gerlach forces and the electromagnetic forces given in Eqs. (53) through (56) can legitimately treated on the same footing, it has implications concerning the relative contribution of magnetic moment and charge to cavity excitation. What makes this valuable for assessing the promise of resonant polarimetry is that there is vast experimental verification of charged particle acceleration by RF cavities.)

possible). Using Eq. (56) and $k_0 c = \omega_0$, for longitudinally polarized particle, the maximum rest frame momentum impulse during one half cycle is

$$\begin{aligned}\Delta p_{0z}^{\parallel \max} c &= c k_0 \int_0^{\pi/\omega_0} \frac{R_{0z}^{m_\parallel TE}(t_0)}{k_0}\, dt_0 \\ &= -j\mu^* B_0 \sin\alpha_0 \cos\alpha_0 \int_0^{\pi} e^{j\omega_0 t_0} d(\omega_0 t_0) \\ &= 2\mu^* B_0 \sin\alpha_0 \cos\alpha_0. \end{aligned} \tag{60}$$

The same calculation for transverse polarization produces

$$\Delta p_{0z}^{\perp \max} c = -2\mu^* B_0 \cos^2\alpha_0. \tag{61}$$

It is important to note the "max" superscripts. These are *maximum possible* momentum impulses due to a single passage through the resonator. The momentum recoil in an electromagnetic wave cannot exceed this amount; but the actual recoil can be much less, even zero (depending on phases). The extreme importance of this comment is emphasized in Section 3.10.

It is important to remember that these are momentum changes, even though they are expressed here in energy units. The overall sign is somewhat arbitrary and can be reversed by shifting the phase by a half cycle. These are "amplitudes" for an eventual superposition over the skew waves making up a resonator mode. As such, their signs are significant and their contributions to the overall coherent sum can be either constructive of destructive.

Values of μ^* are given in Table 4, in units of eV/Tesla. Expressed in momentum units, with B measured in Tesla, Δp_0 is therefore given in units of eV/c.

So far the calculation has been limited to the particle rest frame. In practice the resonant cavity is fixed in the lab frame and the particle is moving through it with relativistic speed V, as illustrated in the lower part of Figure 3. It remains, therefore, to infer the rest frame skew waves from the lab frame skew waves.

3.6. TE_{201} **skew wave superposition.** The momentum impulses given by Eqs. (60) and (61) apply to either of the forward or backward waves for which the forward wave is illustrated in Figure 4. This pair of waves matches the boundary conditions for a horizontal conductive plane perpendicular to the z-axis, but cannot match boundary conditions on a vertical conductoring plane. Other waves are needed to match the side walls of a waveguide. For example, the pair of waves shown in Figure 5 can match boundary conditions on conducting planes parallel to the y, z plane. Though not yet general enough for cylindrical waveguide, this is sufficient for rectangular resonant cavities.

As drawn in the left of Figure 5, one sees that the electric field vanishes on the $x = 0$ plane, and on a set of regularly-spaced planes parallel to that plane. On the z-axis there is a longitudinal magnetic field $B_{0\parallel}$. The vectors for this pair of waves are given in Eqs. (27) through (31). As explained earlier, these waves can either be added or subtracted.

For general rectangular waves the coherent sum is elementary but tedious. Because of their different Lorentz transform behavior, it seems best to perform the Lorentz

transformations wave by wave, rather than summing the skew waves and then transforming. Also, since we are primarily interested in orders of magnitude for now, we continue to accept a single skew wave as typical, though keeping in mind the possibility of total overall destructive interference, producing exactly zero sums.

3.7. Practical parameters. For proton EDM resonant polarimetry, $\beta_{_V} = 0.6$ and $\gamma_{_V} = 1.25$ so the not-fully-relativistic formulation is appropriate. For electron EDM resonant polarimetry, $\gamma_{_V} = 30$, which is relativistic enough for fully-relativistic approximations to apply. Accepting the approximations in Eq. (46), produces $\overline{\alpha} = 1/30 \approx 0.03$. For realistic waveguide modes α is clearly much greater than this. One concludes that the fully-relativistic formulation is adequate for any relevant electron beam polarimetry.

A consideration not mentioned so far has to do with the ratio of resonator length d to particle bunch length σ_z, both being measured in the laboratory. σ_z is likely to range from 1 mm to 10 mm. d is likely to range from 100 mm to 1000 mm. From these ranges, the laboratory ratio d/σ_z can be expected to range from 10 to 10^3. Viewed in the laboratory, σ_z is Lorentz contracted relative to the rest frame bunch length σ_{0z}; that is $\sigma_{0z} = \gamma_{_V}\sigma_z$. On the other hand, viewed from the particle rest frame, the resonator length is Lorentz contracted to $d/\gamma_{_V}$. So the ratio of bunch length to resonator length is greater in the rest frame by a factor of $\gamma_{_V}^2$ compared to the same ratio in the laboratory.

One of the candidate resonant polarimeter tests uses a polarized GeV electron beam at ELSA, for which $\gamma_{_V}^2 > 10^6$. In this case, viewed in the particle rest frame, the resonator length is far less than the bunch length. Curiously enough, there is nothing wrong with this. In an introductory relativity course one encounters the "paradox" of a pole vaulter running through a barn that is shorter than the length of the pole he is carrying. The front door opens just in time to admit the head of the pole and the rear door closes just after the tail enters; the pole hits neither door.

An equivalent situation routinely applies in all high energy accelerators. One cannot, therefore, rule out the test a GeV electron test on the ground of too high $\gamma_{_V}$.

3.8. Resonator excitation due to passing magnetic moment. For a single skew wave, what remains is to calculate the laboratory frame energy losses $\Delta\mathcal{E}_{\parallel}$ and $\Delta\mathcal{E}_{\perp}$ caused by the encounter of a beam particle carrying magnetic dipole moment during a one half period time interval.

Viewed from in its pre-encounter rest frame the particle 4-momentum after the encounter has been changed to $P_0 = (m_p c, \Delta p_{0\parallel}\hat{\mathbf{z}})$. (Rest frame kinetic energy gained by the particle is being neglected.) The corresponding lab frame 4-momentum is $P = (\gamma_{_V} m_p c + \Delta\mathcal{E}/c,\ ,\ ,\ )$, where the spatial components are left blank, both because they are not needed and because momentum imparted to the resonator is not being accounted for. Lorentz transformation back to the lab therefore yields

$$\gamma_{_V} m_p c^2 + \Delta\mathcal{E} = \gamma_{_V}(m_p c^2 + \beta_{_V}\Delta p_{0\parallel} c), \quad \text{or} \quad \Delta\mathcal{E} = \gamma_{_V}\beta_{_V}\Delta p_{0\parallel} c. \tag{62}$$

This treatment has employed an impulse approximation, which presumes $\Delta p_{\parallel} << p_{\parallel}$, which is an overwhelmingly valid approximation in our case.

Applying this formula to the momentum changes obtained in Eqs. (60) and (61), for one hundred percent perpendicular or parallel polarization

$$\Delta\mathcal{E}_{\parallel}^{\max} = 2\gamma_{_V}\beta_{_V}\mu^* B_0 \sin\alpha_0 \cos\alpha_0, \tag{63}$$

$$\Delta\mathcal{E}_{\perp}^{\max} = 2\gamma_{_V}\beta_{_V}\mu^* B_0 \cos^2\alpha_0, \tag{64}$$

$$\tag{65}$$

Here "max" means maximum in absolute value. Also, as has been stated repeatedly, these are the contributions from just one skew wave. The full effect requires a coherent summation over all pairs of skew waves forming the cavity mode.

These quantities still need to be expressed in terms of laboratory variables, using relativistic Doppler shift formulas (33). An especially simple, yet exact, transformation applies for the parallel/perpendicular energy ratio;

$$\frac{\Delta\mathcal{E}_{\parallel}^{\max}}{\Delta\mathcal{E}_{\perp}^{\max}} = \frac{\sin\alpha_0}{\cos\alpha_0} = \tan\alpha_0 = \frac{\sin\alpha}{\gamma_{_V}(\cos\alpha - \beta_{_V})}. \tag{66}$$

As explained earlier, this transformation is qualitatively different in the fully-relativistic and weakly-relativistic cases. We consider the fully relativistic case first.

3.8.1. *Fully-relativistic case.* Repeating Eq. (66) produces

$$\frac{\Delta\mathcal{E}_{\parallel}^{\max}}{\Delta\mathcal{E}_{\perp}^{\max}}\Big|_{\pm} = \frac{\sin\alpha}{\gamma_{_V}(\cos\alpha_{\pm} - \beta_{_V})} = \frac{f_c/f}{\gamma_{_V}(\pm\sqrt{1 - f_c^2/f^2} - \beta_{_V})}, \tag{67}$$

where the "±" refers to forward/backward and, this time, Eqs. (44) have been used to express the skew wave trig functions in terms of waveguide parameters. It is the negative sign option in the replacement of $\cos\alpha$ in the final equation that is specific to the not-very/very relativistic distinction[3]. Since the angle α always lies in the range $0 < \alpha < \pi$, $\sin\alpha$ is always positive. The sign of $\cos\alpha$, on the other hand, reverses from positive to negative as α increases through $\pi/2$, causing $\cos\alpha$ to be positive for forward waves and negative for backward waves. Confirming previous discussion, because the denominator is always negative in the fully-relativistic case, both forward and backward waves in a laboratory waveguide are backward in the rest frame of a beam particle. Setting $\beta_{_V} = 1$, and using approximations (45),

$$\frac{\Delta\mathcal{E}_{\parallel}^{\max}}{\Delta\mathcal{E}_{\perp}^{\max}}\Big|_{\pm} = \frac{\sin\alpha}{\gamma_{_V}(\cos\alpha_{\pm} - \beta_{_V})} \approx \frac{1 - \Delta f/f_c}{\gamma_{_V}(\pm\sqrt{2\Delta f/f_c} - 1)} \approx -\frac{1}{\gamma_{_V}}. \tag{68}$$

Though expressed in the last equation as approximations, the ratios expressed in the first equation are exact. This ratio gives transverse polarimetry an unambiguous $\gamma_{_V}$ magnitude advantage relative to longitudinal polarimetry.

[3]It has been shown, for realistic waveguide parameters, that the denominator expression in Eq. (67) is not particularly singular; the square term can only be close to 1 for frequencies that would, experimentally, be impractically high. In any case, the negative sign of the $\cos\alpha$ term makes the overall denominator factor unambiguously negative, excluding any possibility of singularity. But, if β is not close to 1 (as in the not-very-relativistic regime) then the denominator could be singular, greatly altering the ratio of transverse to longitudinal response. This makes relevant the discussion associated with the space-time behavior of forward and backward waves illustrated in Figure **??**.

To complete the transformation to laboratory parameters, noting from Figure 4 that $B_{0z} = -B_0 \sin\alpha_0$, and using the fact that $B_\parallel$ is invariant,

$$B_z = B_{0z} = -B_0 \sin\alpha_0. \tag{69}$$

can be used. Also (in fully-relativistic approximation)

$$\cos\alpha_{0\pm} = -\sqrt{\frac{1}{1+\tan^2\alpha_{0\pm}}}, \tag{70}$$

showing that both $\cos\alpha_{0\pm}$ values are negative (as has been explained previously). Substituting from Eq. (69) into Eqs. (63) and (64) yields

$$\begin{aligned} \Delta\mathcal{E}_\parallel &= -2\gamma_{_V}\beta_{_V}\mu^* B_z \cos\alpha_0 \quad \approx 2\gamma_{_V}\beta_{_V}\mu^* B_z, \\ \Delta\mathcal{E}_\perp &= -2\gamma_{_V}\beta_{_V}\,\frac{\mu^* B_z}{\sin\alpha_0}\,\cos^2\alpha_0 \approx 2\gamma_{_V}\beta_{_V}\mu^* B_z\,\frac{-1}{\sin\alpha_0}, \end{aligned} \tag{71}$$

The "max" superscripts have been removed since B_z varies sinusoidally. The only remaining rest frame quantity can be replaced using the upper-sign version of Eq. (32)

$$\frac{-1}{\sin\alpha_0} \approx \frac{-1}{\tan\alpha_0} \approx \frac{\gamma_{_V}(1-\cos\alpha)}{\sin\alpha}, \quad \text{where} \quad 0 < \alpha < \pi/2. \tag{72}$$

At this point we can refer back to Figure 4, and to the faint construction on the negative z part of the plot. As drawn, the origin can, if we wish, be interpreted as being located at the entrance to the cavity. Relative to the origin the waves are anti-symmetric and the the electric fields of the forward and backward-going waves cancel exactly at the origin. This is consistent with the $z = 0$ plane being perfectly conductive, which is consistent with this being the entrance to the cavity.

By the same reasoning the origin of the drawing can be interpreted as coinciding with the cavity exit surface. By sliding the faint part of Figure 4 to the right along the z-axis, and the bold part symmetrically to the left, one can produce various superpositions of forward and backward skew waves. For a discrete set of these translations the boundary conditions can be met on both the entrance and exit surfaces of the cavity. In the TE_{mnp} resonant mode designation scheme, say with $m = 2$ and $n = 0$, the only essential distinction among these mode is whether p is odd, as in TE_{201} or even, as in TE_{202}.

As one counter-slides the figures longtudinally, one produces, first, TE_{201}, then TE_{202}, then TE_{203}, and so on. Figure 4 can, with the origin in the figure interpreted as being at the cavity center, corresponds to $p = 21$. It was already shown, in Figure 5, how waveguide modes with different values of mode index m can be produced by superimposing skew wave pairs with opposite-sign α values. These comments can be correlated with the field patterns in Figure 8. In general the resonator width a and depth d need not be rationally related, but we assume that a and d are either equal or their ratio is a small integer.

It is shown in what follows, especially in Section 3.10, for on-axis passage of a polarized beam through such a resonant rectangular cavity, that no net work is done on, or by, the cavity electromagnetic field acting on beam particle magnetic moments. (It is not difficult to conclude this, based on careful interpretation of Eq. (71).) Such a

configuration cannot therefore serve for Stern-Gerlach polarimetry. To overcome this impediment, *slanted beam passage through the cavity is analysed starting in Section 4.*

3.9. Comparison with previous formulations. These formulas for $\Delta\mathcal{E}_{\perp}^{\max}$ and $\Delta\mathcal{E}_{\parallel}^{\max}$ can be compared to formulas for (roughly) the same quantities due to Conte et al.[**2**]. There is agreement as regards the major factors, $\gamma_{_V}^2\mu^* B_{\parallel}$ for perpendicular polarization, and $\gamma_{_V}\mu^* B_{\parallel}$ for parallel polarization. The remaining factors depend on geometric parameters and except for the possibility of exact destructive interference, are dimensionless with numerical values of order 1. For estimating polarimeter performance this is sufficient agreement.

It is shown in this paper, however, that there is, indeed, exact destructive interference, which causes the Conte et al. calculation to be incorrect. This is not original, however; it was already pointed out by Tschalaer. There has been a confusing back-and-forth of communications, starting in 2008 with Tschalaer[**4**][**5**], having to do with the $\gamma_{_V}$ and polarization dependence of the energy dumped in a resonant cavity by the passage through it of a longitudinally polarized beam. This discussion has been superimposed on an ongoing fog of confusion, in (mercifully) unpublished reports, concerning the Lorentz transformation of the magnetic dipole moment 3-vector (a transformation which has been argued here to be meaningless). Also at issue is the effect of end fields on cavity excitation.

Conte paper[**12**] had (in agreement with Eq. (66)) argued that cavity excitation by transverse polarization is greater than by longitudinal polarization by one power of $\gamma_{_V}$, and proposing, therefore, to greatly enhance their Stern-Gerlach effect by intentionally introducing rapid precession of the polarization. Tschalaer showed this to be incorrect; Conte et al. had argued that a certain cancelation did not exist. Tschalaer had disagreed, showing (consistent with my explanation in Section 1) that the same cancelation applied for both transverse and longitudinal excitation. My attitudes concerning this controversy are scattered through this paper.

The confusion had been compounded by ambiguity concerning the effect of RF phase advance between particle entry and exit on the cancelation of terms. Later, in 2009, Conte et al.[**13**] argued that the cancelation in question had been an artifact of their originally incorrect assumption concerning the above-mentioned RF phase advance. In effect this re-affirmed their confidence in their original paper[**2**] (in which discussion of the phase advance is, at best, obscure).

My results agree with Conte, as regards ratio of transverse to longitudinal excitation, but with Tschalaer as regards the dependence on $\gamma_{_V}$ or, more accurately, on the absence a $\gamma_{_V}^2$ enhancement of the $\Delta\mathcal{E}_{\perp}^{\max}$ excitation by on-axis propagation through any cavity.

The situation remains murky for another, more fundamental, reason. The eventual discussions by both Conte et al, and Tschalaer seem to depend on conservation of magnetic energy to calculate the cavity excitation occurring in end fields. Whether any such conservation exists remains at issue.

3.10. Why on-axis cavity beamline orientation cannot succeed. The need for canted resonator is explained in greater detail in this section, which shows why

normal cavity entrance and exit cannot produce Stern-Gerlach cavity excitation. The normal insertion of a rectangular resonator into a beamline is shown top left in Figure 1. Here "normal" is used with two meanings: "expected" and "at right angles". It is the configuration first proposed by Conte et al. for Stern-Gerlach resonance detection. As mentioned earlier, Tschalaer[**4**] disputed the Conte analysis, by demonstrating cancellation to leading order, of the Stern-Gerlach cavity excitation in this configuration. Though this issue has remained controversial for years, the Tschalaer contention seems, by now, to have been accepted.

Much of the discussion on this issue has centered on the influence of "end fields" at cavity entrance and exit, with some demonstrations of the exact cancellation depending on the contributions from the fringe fields. This is somewhat curious in that the cavity aperture can, in principle, be almost infinitesimally small, which might seem to make end fields negligible (as is usually the case with the electric force of cavity fields acting on a passing charge). End fields forces on a magnetic dipole cannot be dismissed so easily though, since the end field forces are large enough to cause energy changes comparable with energy changes in the cavity interior.

Classic Stern-Gerlach force demonstration exhibits transverse separation in a non-uniform DC magnetic field, depending on particle magnetic moment orientation. There is no reason why the DC magnetic field cannot be replaced by a non-uniform RF field to achieve the same separation. It is well known, though, that a transverse force cannot change particle energy. So the RF cavity excitation is not altered by transverse Stern-Gerlach forces.

Only longitudinal force can alter particle energy. There is, however, also a longitudinal Stern-Gerlach force. Equations (59) gives both longitudinal and transverse magnetic dipole response in TE modes. The maximum cavity excitation caused by transverse polarization is given by Eq. (61). The meaning and importance of "maximum" is explained there. The actual cavity excitation is necessarily less than this. In fact it will now be shown, for normal entry and exit, that the excitation necessarily vanishes.

It is convenient to discuss cavity excitation in the frame of reference illustrated in the lower part of Figure 3. It is the particle rest frame at the instant the particle passes the center of the cavity. The reason this frame is convenient is that the particle speed is non-relativistic and non-relativistic formulation is valid. The longitudinal force on a magnetic dipole is proportional to the (longitudinal) derivative of the longitudinal magnetic field.

Consider a plot of $B_{0\|}(z_0)$ versus z_0 as a particle proceeds from entry to exit in the standing wave cavity field. Boundary conditions at entry and exit require $B_{0\|}$ to vanish at both ends. In the simplest case $B_{0\|}(z_0)$ will increase from zero to some extreme value at $z_0 = 0$, and fall symmetrically back to zero at the exit. Meanwhile the particle speed is changing. In fact the origin will be a "turning point" at which the speed vanishes and the orbit reflects. On the graph the deceleration phase retraces the acceleration phase. Because the particle speed is changing, the plot of $B_{0\|}(z_0)$ versus z_0 is not exactly sinusoidal. In the simplest case it will resemble the first quarter period of a sine function.

Because the force is proportional to $dB_{0\|}/dz$, the work done in traveling a distance dz is proportional to the change in $B_{0\|}$ after distance dz. This is the basis for referring to $-\mu^* B_{0\|}(z_0)$ as potential energy. For the complete transit,

$$\Delta B_{0\|} = \int \frac{dB_{0\|}}{dz}\, dz = B_{0\|}^{\text{exit}} - B_{0\|}^{\text{entry}}. \tag{73}$$

Whatever work is done while $B_\|$ is increasing is cancelled as $B_\|$ decreases back to zero. There is also work done in the end fields of the cavity. It is not clear whether the work done on entry contributes to cavity energy but, even if it does, it is exactly cancelled by work done on exit.

For normal entry and exit of a magnetic dipole at nodes of the longitudinal magnetic field, boundary conditions require the separate terms in Eq. (73). each to vanish, which guarantees the field does no work on the particle. There is no such suppression of the work done on an electric charge passing through the electric field in an RF cavity. The work done in this case is proportional to $\int dz\, E_{0\|}$, The entry and exit boundary conditions do not require $E_{0\|}$ to vanish. The integral corresponding to Eq. (73), with $B_{0\|}$ replaced by $E_{0\|}$, is not required to vanish, which makes particle acceleration possible.

Not only is the longitudinal electric field not zero on the entrance and exit faces, it is potentially maximal (though oscillatory). Judiciously entering when the electric field is maximal of one sign, and leaving when the sign is opposite, maximizes the cavity excitation. This is the basis for most RF acceleration.

One has well developed intuition concerning electric potential energy. Its derivative is electric field. What makes magnetic potential energy confusing is the the magnetic field itself (rather than its integral) that is the potential energy.

Resonant cavity magnetic dipole response is therefore disadvantaged, relative to electric, by the boundary condition on entrance and exit faces or the resonator. The boundary condition for electric field is that the electric field has to be normal to the face. The boundary condition for magnetic field is that the magnetic field has to be parallel to the face. In standing wave terminology, the entrance and exit faces have to be nodes of the longitudinal magnetic field. At a node the field vanishes at all times, not just periodically. In particular, the longitudinal magnetic field component vanishes both on particle entry and exit.

Recapitulating, the proper phase interval constraint imposed by entry and exit boundary conditions guarantees zero momentum recoil in the particle rest frame. as a particle moves from entry to exit, it accelerates during the entry half-transit, and decelerates symmetrical during the exit half-transit. There is no net recoil. This is the opposite of "maximum" interaction. The net cavity excitation by on-axis passage of a magnetic moment through a resonant cavity is therefore guaranteed to vanish.

4. Excitation of canted Stern-Gerlach resonator

4.1. Magnetic dipole interaction with individual skew waves. We have to find the work done by a magnetic moment passing through the cavity at slant angle Θ (which is positive by definition). Figure 6 illustrates the four skew wave components

of TE_{20} modes in both the laboratory frame and the rest frame. These waves are identified by ①, ②, ③, ④. To help keep track of the signs of the four rest frame and laboratory angles $\alpha_{0,i}$ and $\alpha_i, i = 1, 2, 3, 4$, which are positive for CCW rotations and negative for CW rotations, we introduce an angle α which is also positive by definition; α is represented by a large font in Figure 6 (rendering the letter at more or less the same size as Θ).

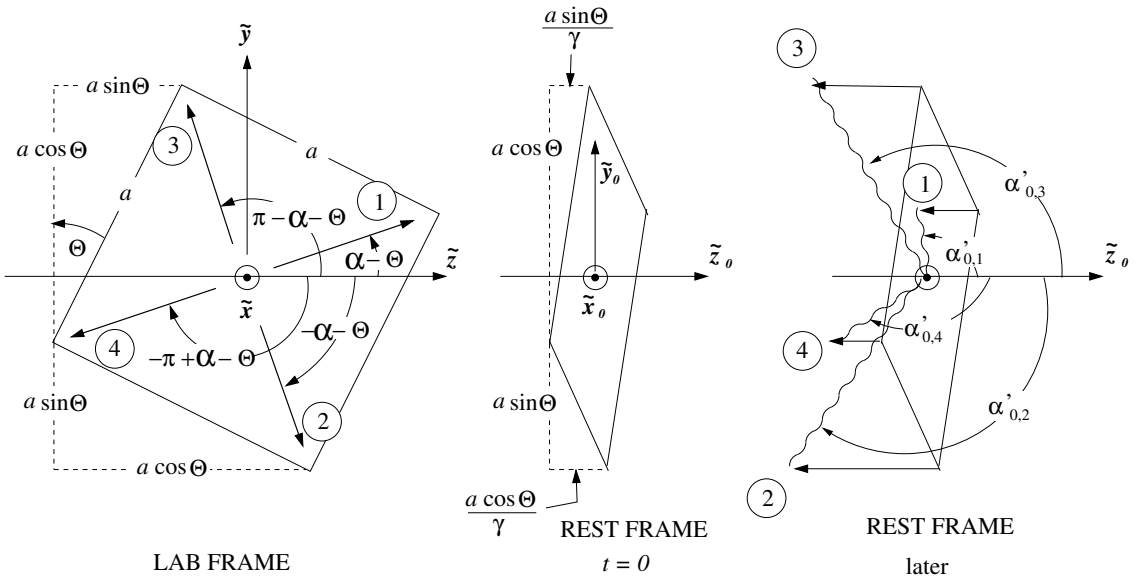

FIGURE 6. Geometry for four skew waves in TE_{202} resonator, canted by angle $\Theta = 26.57°$, with forward and backward laboratory skew wave angles $\pm 45°$. The mode field is constructed from the four skew waves shown. Parameters are given in Table 2. The middle figure is a rest frame snapshot at $t_0 = 0$. Though square in the laboratory, the cavity is a parallelogram in the rest frame. The right hand figure shows the four corners at a slightly later time to indicate the four wave vector directions which are positive for CCW rotations and negative for CW. Large font quantities α and Θ are positive by definition.

Rest frame forces due to direct beam charge in TM modes, and to longitudinal and transverse magnetic dipole moment vectors have been determined (for on-axis traversal) in Section 3.5. We now repeat the calculation, assuming this time that the beam is slanted by angle Θ relative to the resonator axis. In the laboratory frame, for a skew wave with angle α relative to the cavity axis, angle α' relative to the particle path is given by

$$\alpha' = \alpha - \Theta. \tag{74}$$

Previously-derived rest frame force formulas can now be employed with $\alpha_0 \to \alpha'_0$. The rest frame angle α'_0 corresponding to laboratory angle α' has to be found using a

relativistic Doppler shift formula. Copying from Eq. (59), for a skew wave at angle α'_0 in the rest frame, the forces are:

$$F_{0z'}^{eTM} : R_{0z'}^{m_\parallel TE} : R_{0z'}^{m_\perp TE}$$
$$= -eE'_{0z'}\, e^{j\omega'_0 t_0} : -jk'_0(\mu^* B'_0)\, \sin\alpha'_0 \cos\alpha'_0\, e^{j\omega'_0 t_0} : jk'_0(\mu^* B'_0)\, \cos^2\alpha'_0\, e^{j\omega'_0 t_0}. \quad (75)$$

Lorentz transformation from laboratory to rest frame is illustrated in Figure 6. For the sake of concreteness and definiteness, especially as regards signs, we use definite numerical values $\Theta = 26.57°$. Numerical values for this example are tabulated in Table 2 and Table 3. Subscript "0" signifies rest frame, and primes indicate skew path through the resonator. The canted geometry affects this transformation significantly.

The directions of the four skew waves in the rest frame are designated as $\alpha'_{0,i},\ i = 1, 2, 3, 4$; and similarly for $\omega'_{0,i}$, $k'_{0,i}$, $B'_{0,i}$, $E'_{0,i}$ and the force components. From Eqs. (33) and (69) we have

$$\omega'_{0,i} = \gamma_V \omega(1 - \beta_V \cos\alpha'_i) \approx \gamma_V \omega(1 - \cos\alpha'_i), \quad (76)$$
$$k'_{0,i} = \gamma_V k(1 - \beta_V \cos\alpha'_i) \approx \gamma_V k(1 - \cos\alpha'_i), \quad (77)$$
$$\alpha'_{0,i} \approx \tan\alpha'_{0,i} = -\frac{\sin\alpha'_i}{\gamma_V(\beta_V - \cos\alpha'_i)} \approx -\frac{\sin\alpha'_i}{\gamma_V(1 - \cos\alpha'_i)}, \quad (78)$$
$$B'_0 = \gamma_V(1 - \beta_V \cos\alpha'_i)\, B \approx \gamma_V(1 - \cos\alpha'_i)\, B. \quad (79)$$

For the appoximate versions here we are assuming that $\gamma_V >> 1$, so $\beta_V \approx 1$, and that α'_i is not close to zero or to $\pm\pi$. As a result the $(1 - \cos\alpha'_i)$ approximations respect the signs of the quantities they replace.

In the rest frame, at position $z_0 = 0$, the wave phases depend only on time, $\phi'_{0,i} = \omega'_0 t_0$. The entrance to exit proper phases, divided by 2, are

$$\frac{\Delta\phi_{0,i}}{2} = \frac{\omega'_{0,i}\big(t_0(\text{exit}) - t_0(\text{entry})\big)}{2}. \quad (80)$$

$\phi'_{0,i}$ is referred to as "proper phase advance" because the particle is physically present at both start and end of the time interval in question.

To convert from force to momentum impulse requires the integration over time of these forces. The required integral is

$$c\int e^{j\omega'_{0,i}t_0}\, dt_0 = \frac{c}{\omega'_{0,i}} \int_{\text{entry}}^{\text{exit}} (\cos\omega'_{0,i}t'_0 + j\sin\omega'_{0,i}t'_0)\, d(\omega_{0,i}t'_0) = \frac{2}{k'_{0,i}} \int_0^{\text{exit}} \cos\phi'_{0,i}\, d\phi'_{0,i}. \quad (81)$$

For transverse polarization, integrating the third of Eqs. (75),

$$c\Delta p_{0z'}^{m_\perp TE} = j(\mu^* B'_0)\, \cos^2\alpha'_0\, 2 \int_0^{\text{exit}} \cos\phi'_{0,i}\, d\phi'_{0,i}$$
$$= j(\mu^* B'_0)\, \cos^2\alpha'_0\, 2\, \sin\frac{\Delta\phi_{0,i}}{2}, \quad (82)$$

and the other two terms in Eqs. (75) can be processed the same way. The laboratory cavity excitation strengths can then be obtained using Eq. (62); multiplying all expressions in Eq. (75) by the factor $\gamma_V\beta_V$ converts from rest frame momentum to laboratory

energy excitations;

$$\Delta\mathcal{E}^{eTM}_{i,z'} = \gamma_V\beta_V\,\frac{-eE'_{0z'}}{k'_0}\,2\,\sin\frac{\Delta\phi_{0,i}}{2},$$
$$\Delta\mathcal{E}^{m_\parallel TE}_{i,z'} = -j\gamma_V\beta_V\,(\mu^* B'_0)\,\sin\alpha'_0\cos\alpha'_0\,2\,\sin\frac{\Delta\phi_{0,i}}{2},$$
$$\Delta\mathcal{E}^{m_\perp TE}_{i,z'} = j\gamma_V\beta_V\,(\mu^* B'_0)\,\cos^2\alpha'_0\,2\,\sin\frac{\Delta\phi_{0,i}}{2}. \tag{83}$$

Because wave phases are invariant from frame to frame, the phase advances $\Delta\phi_{0,i}$ are the same in lab and rest frames, but this does not mean they are the same for the four skew waves; that is, $\Delta\phi_{0,i}$ depends on i. For each value of "i", $\Delta\phi_{0,i}$ can be replaced by $\Delta\phi_i$ and evaluated in the laboratory. The evaluation of $\Delta\phi_i$ was explained in Section 3 as skew waves were first being introduced.

TABLE 2. Skew wave geometry of the four skew waves forming the TE_{202} mode, for which $\alpha = 45°$. Unprimed variables are measured relative to the cavity axis, primed variables are measured relative to the beam orbit, which passes through the cavity at slant angle $\Theta = 26.57°$. The rest frame angles α'_0 are obtained using the final approximation of Eq. (78). The laboratory wave number k has a numerical value of order $10\,\mathrm{m}^{-1}$. Large font quantities α and Θ are positive by definition.

ray number	α degree	α'	α' degree	$\sin\alpha'$	$\cos\alpha'$	$1-\cos\alpha'$	$\alpha'_0 - \frac{\sin\alpha'}{\gamma_V(1-\cos\alpha')}$ radian
1	45	$\alpha'_1 = \alpha - \Theta$	18.43	.3162	.9487	0.05132	-6.16228/γ_V
2	-45	$\alpha'_2 = -\alpha - \Theta$	-71.57	-.9487	.3162	0.68377	1.38743/γ_V
3	135	$\alpha'_3 = \pi - \alpha - \Theta$	108.43	.9487	-.3162	1.31623	-0.72076/γ_V
4	-135	$\alpha'_4 = -\pi + \alpha - \Theta$	-161.57	-.3162	-.9487	1.94868	0.16228/γ_V

TABLE 3. Continuation of Table 2 The "amplitude(i)" entries in the final column are values of the coefficient $(1-\cos\alpha'_i)\,2\,\sin\left(\frac{\pi}{\sqrt{2}}\,\frac{1-\cos\alpha'_i}{\cos\theta}\right)$ in Eq. (87). As signed amplitudes, their sum gives the coefficient of the overall cavity excitation.

ray number	α degree	α'_0 radian	$1-\cos\alpha'$	$\Delta\phi_0/2$ $\sin\left(\frac{\pi}{\sqrt{2}}\,\frac{1-\cos\alpha'}{\cos\theta}\right)$	k'_0 1/m	B'_0	amplitude(i)
1	45	-6.16228/γ_V	0.05132	0.12711	51.317 k	51.317 B	0.01305
2	-45	1.38743/γ_V	0.68377	0.9919	683.77 k	683.77 B	1.35645
3	135	-0.72076/γ_V	1.31623	-0.12711	1316.2 k	1316.2 B	-.33461
4	-135	0.16228/γ_V	1.94868	-0.9919	1948.7 k	1948.7 B	-3.86576
sum							-2.83086

(The entries in Table 3 show that there is a sense in which it is most "natural" to treat skew waves 1 and 3 as one pair, and 2 and 4 as the other. Except for sign, the

proper phase intervals of 1 and 3 are the same. Similarly, the proper phase intervals of 2 and 4 are equal and opposite. This should probably be considered to be a coincidence, however. We have assumed that resonator width and depth are the same (or in the ratio of small integers). This is why the four skew wave angles are multiples of 45 degrees. But the symmetry of proper phase intervals depends on our choice of angle Θ (such that $\tan\Theta = 1/2$) which was somewhat arbitrary.)

Containing quantities in both rest frame and laboratory frame, Eqs. (83) are in a kind of hybrid form. The rest frame quantities B'_0 and α'_0 need to be expressed in terms of lab frame quantities using Eqs. (76) through (79). Numerical values for the TE_{202} mode example are given in Table 2 and Table 3. According to Eq. (24), the proper phase interval from particle passage through the midpoint of the cavity to its exit is given by

$$\Delta\phi_{\alpha,\theta}(d/2) = \frac{kd/2}{\cos\theta}\left(\frac{1}{\beta_{_V}} - \cos(\alpha-\theta)\right) \approx \frac{kd/2}{\cos\theta}\left(\frac{1}{\beta_{_V}} - \cos\alpha'\right) \tag{84}$$

For our numerical example, $\lambda = \sqrt{2}d$, so $kd/2 = \pi/\sqrt{2}$. In fully relativistic approximation, using $\cos\alpha'_0 \approx 1$, and approximating $\sin\alpha'_0$ using Eq. (78),

$$\Delta\mathcal{E}^{eTM}_{i,z'} \approx \beta_{_V}\,\frac{-eE'_{0z'}}{k(1-\cos\alpha'_i)}\,2\,\sin\left(\frac{\pi}{\sqrt{2}}\,\frac{1-\cos\alpha'_i}{\cos\theta}\right), \tag{85}$$

$$\Delta\mathcal{E}^{m_\parallel TE}_{i,z'} \approx j\gamma_{_V}\beta_{_V}\,\mu^*B\sin\alpha'_i\,2\,\sin\left(\frac{\pi}{\sqrt{2}}\,\frac{1-\cos\alpha'_i}{\cos\theta}\right), \tag{86}$$

$$\Delta\mathcal{E}^{m_\perp TE}_{i,z'} \approx j\gamma_{_V}^2\beta_{_V}\,\mu^*B(1-\cos\alpha'_i)\,2\,\sin\left(\frac{\pi}{\sqrt{2}}\,\frac{1-\cos\alpha'_i}{\cos\theta}\right). \tag{87}$$

For transverse beam polarization, the coefficient in the sum over the four skew waves, $\sum_{i=1}^{4}\Delta\mathcal{E}^{m_\perp TE}_{i,z'} = -2.83$ is given in the last row of the table. This coefficient multiplies the $j\gamma_{_V}^2\beta_{_V}\,\mu^*B$ factor in Eq. (87). The individual numerical values in the last row of the table can be compared with the coefficient "2" in the second of Eqs. (71), which was the result of a less detailed, approximate calculation.

The estimate of the direct background due to electric charge excitation remains incomplete in that expressing $E'_{0z'}$ in lab frame quantities has not yet been performed. If $\mathbf{E'_0}$ were purely longitudinal then $E'_{0z} = E'_\parallel$ but, with the resonator being canted, there is a substantial transverse electric component. Fortunately only rough estimates of $\Delta\mathcal{E}^{eTM}_{i,z'}$ values are needed.

These equations differ from Eqs. (59) primarily because they allow angles α' to be measured from a "primed axis" which deviates from the resonator axis by an angle Θ. Furthermore, integration over realistic (rather than maximal) phase interval has been performed.

The magnetic dipole vector components are now referred to the slanted beam path. In particular, the primed axes do not align with the entrance and exit planes of the resonator. Of course this was the entire motivation for introducing the slanted axis. Fixed standing wave nodes are still guaranteed on entrance and exit for magnetic field normal to the surfaces, but the surfaces are anti-nodes for magnetic field parallel to the surfaces, which now have non-zero components along the beam direction.

4.2. Dominant single skew wave approximation? For any of the TE_{20p} series of resonator modes the cavity excitation is the superposition of the amplitudes from just the four skew waves analysed in this paper. These skew waves are represented by the wave vectors shown in Figure 6. The beam path is along the z-axis but the cavity is slanted by angle Θ. For an on-axis beam the four waves would consist of left/right symmetric pairs of forward/backward pairs of skew waves. Lorentz transformation spoils the forward/backward symmetry but preserves left/right symmetry. Slanted beam passage through the resonator also spoils the left/right symmetry. This makes it possible that just one of the four skew waves might dominate the Stern-Gerlach resonator excitation. This would be especially attractive for preliminary planning purposes, because the possibility of near-perfect destructive interference hazard would be, because semi-quantitative accuracy is all that is being sought, and because simplicity is reassuring. One sees, from Table 3, that skew wave 4 is dominant in this sense.

5. Resonator for Stern-Gerlach polarimetry test

5.1. Rectangular resonant cavities. Most of this section is drawn from Ramo, Whinnery, and Van Duzer[**9**]. Cylindrical TE_{11} modes were, for a while, the favored resonator type for resonant polarimetry. However, for reasons of symplicity, only rectangular resonator excitation has been analysed in this paper. By referring to the mode patterns shown in Figures 8 and 11 one can see that (for on-axis beams) the rectangular TE_{20} mode quite closely resembles the cylindrical TE_{11} mode—even if the subscripts suggest otherwise. This led to the experimental configuration shown in Figure 1. The beam enters the cavity at right angles to the cavity. This has been referred to previously as "normal" entry and exit.

As explained in this paper, normal entry geometry has now been ruled out. It has been shown, for on-axis passage, no energy can be coupled from polarized beam to cavity. The way I propose to overcome this impediment is shown at the top right of Figure 1. The beam travels somewhat diagonally across the cavity, at angle Θ relative to the z-axis. For now I consider the canted-TE_{20} sequence of resonators of increasing length, as the most promising choices for Stern-Gerlach polarimetry. For most of this section the proposed slanted beam path through the resonator is not important. None of the cavity properties will depend on the cant angle Θ.

Earlier explanations of constructing waveguide modes from skew waves have been aimed toward producing TE_{10} and TE_{20} rectangular modes. The field patterns for these modes are shown in Figure 8, and the forward skew wave pairs are shown in Figure 5: TE_{10} on the left; TE_{20} on the right. The same two skew waves can form either mode, depending on the placement of the waveguide walls; or, equivalently, with different placement of the z-axis. (A vertical conducting plane along the z-axis of the TE_{20}, in effect, produces two TE_{10} guides, parallel-connectd, side-by-side. It may take a while staring at the figures for these statements to be understandible.)

The TE_{10} mode has vanishing longitudinal magnetic field on-axis, which is not satisfactory for our purposes. However, the TE_{20} mode has non-zero longitudinal magnetic field on axis. This mode also has transverse electric and magnetic fields on-axis. Though not helpful for resonance excitation, it has been shown earlier that

the presence of these fields can help to solve another knotty problem—how to read out the resonator excitation. The suggested answer is "by sensing the betatron excitation caused by the mode excitation".

One is always reluctant to build a high Q resonator into a accelerator vacuum chamber. It threatens to "blow the impedance budget". If this cannot be avoided the peak current will be limited. But, as well as being optimized for MDM sensitive, the proposed cavity is designed to not couple directly to the beam charge. It should also be somewhat helpful that the beam line vacuum chamber and resonator heights have been chosen equal in Figure 1.

There are good reasons for the rectangular resonator to be so much wider than it is high. In the ideal situation the lowest resonator TE mode is below cut-off in the ring vacuum chamber and the lowest resonator TM mode is above cut-off in the ring vacuum chamber. The resonator TE mode can then have high Q, while any insipient TM mode excitation by the beam charge is rapidly damped by leakage into the rest of the ring vacuum chamber.

Cut-off frequencies for both TE_{mn} and TE_{mn} rectangular waveguides are given by

$$f_c(m,n) = \frac{c}{2}\sqrt{\frac{m^2}{a^2} + \frac{n^2}{b^2}}. \tag{88}$$

For example,

$$f_c(\mathrm{TE}_{m0}) = \frac{c\,m}{2a},\ f_c(\mathrm{TM}_{11}) = \frac{c\sqrt{1+a^2/b^2}}{2a},\ \frac{f_c(\mathrm{TE}_{m0})}{f_c(\mathrm{TM}_{11})} = \frac{m}{\sqrt{1+a^2/b^2}}. \tag{89}$$

Notice that for TM modes, neither m nor n can be zero. This prejudices the lowest TM cut-off frequencies to be larger than TE cut-off frequencies. (For fixed a and b) there is a penalty (proportionally in increased cut-off frequency) for TE mode, of increasing m from 1 to 2. But there can be a more than compensating increase in TM frequency proportional to $\sqrt{1+a^2/b^2}$ of increasing the a/b ratio. By increasing the resonator width to height ratio to 4, the TE_{20} resonator shown in Figure 1 has lower cut-off frequency than the lowest TM mode. (Trying to visualize these modes as lumped LC circuits, reducing beam height b increases capacity C more or less inversely for a TE mode, tending to reduce its resonant frequency. But there is a less than proportional increase in inductance L resulting from increasing the beam width a.)

It is this calculation, along with matching the resonator height to the connecting waveguide height, that fixes the transverse resonator dimensions. If necessary, d can be increased to further desensitize against direct beam charge excitation. The cut-off frequencies can be scaled up or down by changing all transverse dimensions inversely.The resonator length is fixed by the choice of f/f_c.

5.2. Stern-Gerlach signal induced in square pancake-shaped resonator. According to page 545 of Ramo et al.[**9**], the quality factor of a flat ($b << a$) square ($a = d$) cavity is given by

$$Q_{\mathrm{sq.p.}} \approx \frac{\pi\eta}{4R_s}\,2\sqrt{2}\,\frac{b}{a} \approx 0.28\,\frac{\eta}{R_s}\sqrt{\frac{10}{f_r[\mathrm{GHz}]}}, \tag{90}$$

where $\eta = 377\,\text{ohm}$ and, for room temperature copper, at 10 GHz, the surface resistance is $R_s = 0.0261\,\text{ohm}$ at 10 GHz. For the $b/a = 0.125$ cavity dimensions shown in Figure 1, $Q^{\text{Cu}}_{\text{sq.p.}} = 4010$. (For different resonant frequency f_r the Q value scales as $1/\sqrt{f_r}$). For peak vertical electric field E_0 the electromagnetic energy stored in the cavity is given by

$$U_{\text{sq.p.}} = \frac{abd\mu_0}{8} H_\parallel^2, \quad \left[\frac{\text{Jm}^2}{\text{A}^2}\right]\left[\frac{\text{A}^2}{\text{m}^2}\right]. \tag{91}$$

(The units of $H_\parallel$ are [A/m].) For the present calculation we suppose that the cavity is being externally driven, with power P^{ext} at exactly the cavity resonant frequency f_r. The quantities introduced so far are related by

$$P^{\text{ext}} = \frac{\omega_r U_{\text{sq.p.}}}{Q_{\text{sq.p.}}} = \frac{2\pi f_r\,\mu_0 H_\parallel^2}{Q_{\text{sq.p.}}}\,\frac{abd}{8}. \tag{92}$$

This equation can be re-arranged to express $H_\parallel$ in terms of the P^{ext};

$$H_\parallel = \sqrt{\frac{Q_{\text{sq.p.}}}{2\pi f_r}\,\frac{8}{abd\mu_0}\,\frac{1}{P^{\text{ext}}}}\,P^{\text{ext}}, \quad \sqrt{[\text{s}]\left[\frac{\text{A}^2}{\text{Jm}^2}\right]\left[\frac{\text{s}}{\text{J}}\right]}\,\left[\frac{\text{J}}{\text{s}}\right], \tag{93}$$

where $\sqrt{P^{\text{ext}}}$ has been multiplied and divided for convenience in the next step.

Consider a one hundred percent (transversely) polarized bunched electron beam with beam current $I_e \overset{\text{e.g.}}{=} 10^{-4}\,\text{A}$, and repetition rate $f_0 \overset{\text{e.g.}}{=} 0.5\times 10^9\,\text{Hz}$. The number of electrons per bunch is

$$N_e = \frac{I_e}{eN_e} \overset{\text{e.g.}}{=} \frac{10^{-4}}{(0.5\times 10^9)\cdot(1.6\times 10^{-19})} = 1.25\times 10^6\,\text{electrons/bunch}. \tag{94}$$

According to Eq. (4) the passage of transversely polarized electrons also supplies power to the cavity. The power is

$$P^{\text{SG}} = f_0 N_e \mathcal{P}(\Theta)\gamma_v^2\mu_e^*\mu_0 H_\parallel; \quad \left[\frac{1}{\text{s}}\right]\left[\frac{\text{J}}{\text{T}}\right]\left[\frac{\text{T}\cdot\text{m}}{\text{A}}\right]\left[\frac{\text{A}}{\text{m}}\right]. \tag{95}$$

where $P(\Theta)$ is a "penalty function" whose value is less than 1. Substituting from Eq. (93) into this equation, and dividing by P^{ext} produces

$$\frac{P^{\text{SG}}}{P^{\text{ext}}} = f_0 N_e \mathcal{P}(\Theta)\gamma_v^2\mu_e^*\,\mu_0\sqrt{\frac{Q_{\text{sq.p.}}}{2\pi f_r}\,\frac{8}{abd\mu_0}\,\frac{1}{P^{\text{ext}}}}, \quad \left[\frac{1}{\text{s}}\right]\left[\frac{\text{J}}{\text{T}}\right]\left[\frac{\text{T}\cdot\text{m}}{\text{A}}\right]\sqrt{[\text{s}]\left[\frac{\text{A}^2}{\text{Jm}^2}\right]\left[\frac{\text{s}}{\text{J}}\right]}. \tag{96}$$

5.2.1. *Parameter values .*

$$\begin{aligned}
\text{bunch frequency } f_0 &= 0.5\times 10^9\,\text{Hz},\\
\text{beam current } I_e &= 100\,\mu\text{A},\\
\text{electrons/bunch } N_e &= 1.25\times 10^5,\\
\text{penalty function} &= 0.25,\\
\text{electron energy} &= 123\,\text{MeV},\\
\text{relativistic gamma} &= 241,\\
\text{electron magnetic moment} &= -0.928\times 10^{-23},\ \text{J/T},\\
\text{Resonator Q}-\text{value} &= 10^4,\\
\text{resonator frequency} &= 1.0\,\text{GHz},\\
\text{resonator dimensions } a/b/d &= 0.4/0.05/0.4\,\text{m}\\
\frac{a\,b\,d\,\mu_0}{8} &= 1.26\times 10^{-9}\,\frac{\text{J}}{(\text{A/m})^2},\\
\sqrt{\frac{Q_{\text{sq.p.}}}{2\pi f_r}\,\frac{8}{abd\mu_0}\,\frac{1}{P^{\text{ext}}}} &= \frac{40.1}{\sqrt{P^{\text{ext}}}},\\
\frac{P^{\text{SG}}}{P^{\text{ext}}} &= \frac{-4.23\times 10^{-9}\,\sqrt{\text{W}}}{\sqrt{P^{\text{ext}}\,[\text{W}]}}.
\end{aligned} \tag{97}$$

6. Room temperature S-G polarimetry test at CEBAF

The S-G signal is extremely weak compared to direct beam charge excitation. The cleanest way to extract the S-G signal is for its frequency to differ from the frequency of the charge signal. This makes it essential to shift the S-G frequency away from the beam repetition frequency. In a storage ring it is possible to exploit the spin tune precession to perform this frequency shift.

In a linear accelerator, the fact that each bunch passes the S-G resonator only once, makes it hard to arrange for the polarization of successive bunches to be different. It can ony be done at the electron source, either by alternating the (circular) polarization of the laser of the photo-injector, or by swinging the electron polarization at the front end of the injector line where the electron energy is still quite low. The frequency with which the bunch polarization oscillates is thought to be limited to, perhaps, 10 kHz, which corresponds to a polarization oscillation period of $T_{\text{pol}} = 100\,\mu\,\text{s}$.

The Stern-Gerlach resonant cavity can serve as a filter to separate the S-G signal from the direct charge signal, based on their different frequencies. For best cancellation of the direct charge excitations, the cavity oscillates with constant amplitude for time long enough at the S-G frequency for the direct excitation to fall out of phase by an amount large compared to 2π. For best separation one wants the Q-value of S-G resonator to be high. For ultimate performance this will require a cryogenic superconducting cavity. But we have already accepted that the first test should use a room temperature cavity. For frequency such as $f_r \approx 1\,\text{GHz}$, one expects, for example, $Q_r \approx 10^4$.

This corresponds to a resonator damping lifetime of about $T_{\rm damp} \approx 10\,\mu$s, which is small compared to the polarization oscillation period. The fact that $T_{\rm damp} << T_{pol}$ largely defeats the filtering action—the beam polarization does not change rapidly enough.

In the extraction beam line of CEBAF, which is a recirculating linac, a single bunch can, similarly, pass through the S-G resonator only once. But now adjacent A and B bunches (coming in the sequence A,B,A,B,$\cdots$, can have different energies (because of their different number of recirculations). Furthermore, because of their different histories, adjacent bunches can be arranged to have arbitrarily different polarizations, for example both purely transverse, but of opposite sign. Since the bunch repetition rate is of order 1 GHz, the number of S-G resonator cycles during damping time $T_{\rm damp} \approx 10^{-5}\,$s is of order 10^4.

This makes possible a huge suppression of direct charge excitation relative to S-G excitation. There are however, effects that limit the effectiveness of this suppression. There will be an r.m.s. deviation σ_{AB} between the A and B bunches. Furthermore, to the extent the S-G resonator is tipped vertically by r.m.s. angle σ_{Θ_v}, the benefit that the S-G cavity resonates in a TM mode (insensitive to passing beam charge) is defeated.

Figure 7 illustrates such a CEBAF-like bunch train, passing through the S-G resonator. Table 1, introduced earlier in the paper, gives the enhancement of the S-G signal relative to the direct charge signal, coming from $\Delta f/f$ filtering and other experimental design features. Since bunch B has twice the energy of bunch A, its S-G signal is four times greater. But, more to the point, its dominant frequency is f_r=500 MHz, half as great as the bunch frequency, whose dominant, and lowest, frequency is f_0=1000 MHz.

Comparison of TE and TM mode cut-off frequencies are discussed in connection with Eq. (89). By decreasing the b/a ratio the frequencies of TM modes are moved to high frequencies. This is favorable for S-G polarimetry since beam magnetization excites TE modes, while beam charge excites TM modes.

The cut-off frequency in a rectangular waveguide, with horizontal mode index m, and vertical mode index $n = 0$ is given by

$$f_c = \frac{c}{2}\,\frac{m}{a}. \tag{98}$$

Consider a rectangular cavity with dimensions, as defined in Figure 1, a^r=0.424 m, b^r=0.05 m, d^r=0.424 m. For the $\rm TE_{202}$ resonant mode with these dimensions the parameters are

$$\begin{aligned} \text{resonant frequency, } f_r &= \frac{c}{\lambda} = 0.5\,\text{GHz}, \\ \text{free space wavelength, } \lambda_r &= \frac{c}{f_r} = 0.6\,\text{m}, \\ \text{guide wavelength, } \lambda_g^r &= \lambda/\sqrt{2} = 0.424\,\text{m}. \end{aligned} \tag{99}$$

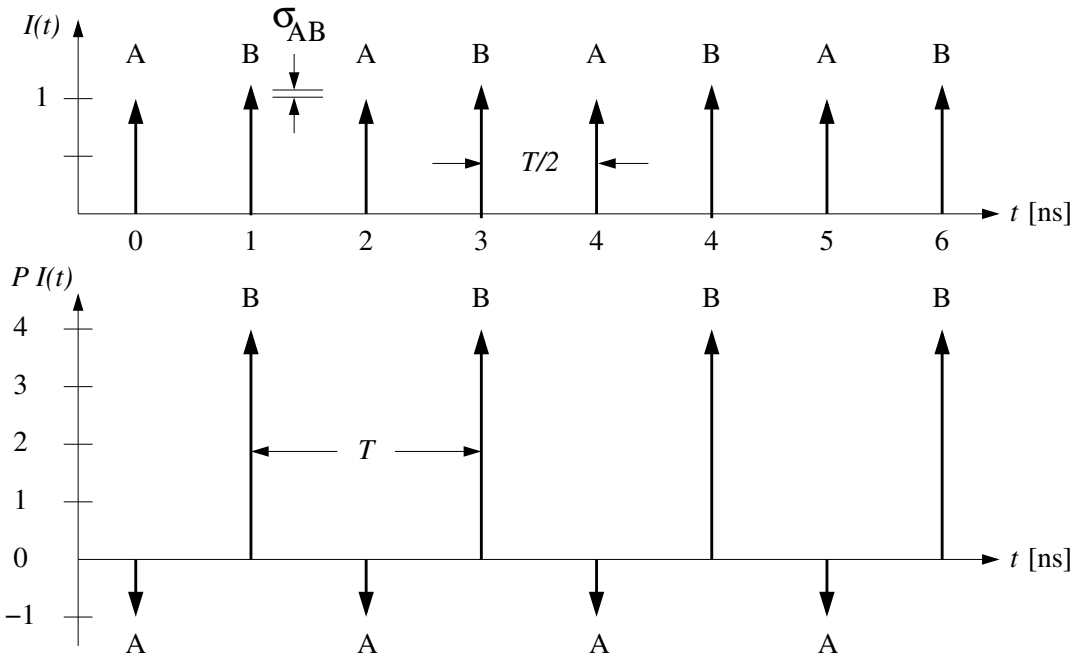

FIGURE 7. Beam current $I_e(t)$ pulses (above) and beam magnetization $P\,I(t)$ (pulses (below) for a possible CEBAF extraction line test of Stern-Gerlach resonant polarimetry. (Though shown as 1 GHz, the actual bunch repetition frequency would be 1.5 GHz.) Beam bunches A, with energy $\mathcal{E}_A$ and effective S-G strength $\mathcal{S}_A = -1$, are interleaved with B-bunches of energy $\mathcal{E}_B = 2\mathcal{E}_A$ and S-G strength $\mathcal{S}_B = 4$.

The parameters for the adjacent waveguide connections are a^{bl}=0.180 m, b^{bl}=0.05 m. The cut-off frequency for such a waveguide is given by

$$\text{cut} - \text{off frequency, } f_c^{bl} = \frac{c}{2a} = 0.833\,\text{GHz}, \tag{100}$$

This value of beam-line cut-off frequency is high enough that the cavity cannot oscillate losslessly at the bunch train frequency or at any harmonic of that frequency—these are the frequencies present in the upper plot of Figure 7. However the resonator can oscillate with high Q_r-value at the 0.5 GHz S-G frequency of the beam magnetization.

7. Experimental considerations

7.1. Separating MDM and direct charge excitation frequencies. Resonant excitation by MDM has mainly been discussed. An issue likely to be just as important is the spurious excitation that will be caused by direct cavity excitation caused by the beam charge. As has been stated repeatedly, resonant polarimetry favors the so-called TE modes because their vanishing laboratory frame longitudinal electric field eliminates

the leading source of direct coupling to beam charge.[4] The leading way of reducing this "background" source is to consider only TE modes for resonant polarimetry. With no longitudinal electric field TE modes do not couple directly to the beam charge. In this paper I therefore emphasize TE modes, expecting to pick the TE mode of lowest frequency f_r as the frequency tuned to the frequency with which the magnetization of the passing beam oscillates. In a cylindrical waveguide this mode is of TE_{11} type, but rectangular cavities are shown later to be more appropriate than

The most important parameter influencing the foreground to background ratio is the frequency difference between the bunch frequency and the magnetization frequency. In the eventual EDM experiment these frequencies will probably have to be quite close. But, for first demonstrating the resonant polarimeter principle, it should be possible to move the MDM frequency well away from any harmonic of the revolution frequency, in order to improve foreground to background ratio. In any case, the two measures of ease of suppressing direct excitation are large frequency difference Δf and large resonator Q-value.

The polarization vector of a vertically polarized beam in a storage ring survives more or less indefinitely. But, passing such a beam through a resonator cavity, the MDM excitation frequency is automatically a harmonic of the revolution frequency. The simplest polarized linac beam configurations have the same property. In either storage ring or linac the beam has to be specially tailored to move the Stern-Gerlach magnetization frequency away from the bunch repetition frequency.

There is a natural way to shift the MDM frequency away from harmonics of the revolution frequency in a electron storage ring such as ELSA. It is to impulsively rotate the natural vertical polarization into the horizontal plane as rapidly as possible. From this condition every particle will precess relative to the orbit direction at spin tune (i.e. frequency) $G_e\gamma$. For electrons, with $G_e = 0.00116$ and, for example, $\gamma_{_V} = 2000$. the spin $G_e\gamma_{_V}$ precession rate and the revolution frequency are therefore comparable. By varying $\gamma_{_V}$ the forground and background frequency difference can be regarded as arbitrarily adjustable. This is ideal for separating the Stern-Gerlach frequency from the nearest revolution harmonic.

After rotation of all spins into the horizontal plane, the presence of beam energy spread would tend to cause the polarization of a coasting beam to decohere rapidly, for example in milliseconds. But the beam will, in fact, be bunched, and synchrotron oscillations will, to a first approximation, suppress the decoherence, extending the spin coherence time (SCT), to perhaps several seconds. With further effort, for example sextupole family tuning, SCT may be further increased. This possibility needs to be analysed using a particle and spin tracking code such as ETEAPOT[**15**][**16**].

---

[4]Our concentration on only TE modes differs from Derbenev[**1**] who concentrated on a single TM mode. This different emphasis is based purely on my concern about the experimental difficulties imposed by longitudinal electric fields present with TM modes; because of their non-zero electric fields, these modes couple directly to beam charge, which presents an experimental complication. Otherwise the choice between TE and TM modes is qualitatively immaterial for the essential issues discussed in this paper.

Eventually, the Stern-Gerlach resonator will be superconducting, and extremely high Q-values will be achievable. If the resonator frequency is, say, 1 GHz, then there will be 10^9 cycles per second and the ring-up time for $Q = 10^9$ will be a few seconds. This can be fully effective only if the beam SCT value exceeds a few seconds. These parameters can be used as parameter choices for obtaining "ball-park" estimates of achievable polarimeter performance.

An ideal resonator would have a single mode that can be excited by the magnetic dipole of a passing charge, but not by the charge itself. Unfortunately, in reality, a microwave cavity has many resonant modes, of both TE and TM type, starting from some lowest cut-off frequency and extending to arbitrarily high frequency. In a cylindrical resonator the mode lowest in frequency is TE_{11}, followed by TM_{01}. The order of cylindrical mode frequencies is given in detail in Figure 9. In a rectangular waveguide the lowest frequency mode is TE_{10} (See Figure 8.)

Having picked the lowest frequency TE mode as "foreground" and the lowest TM mode as "background" the task is to further minimize the direct charge response relative to the MDM response. We assume the MDM frequency ω_r can be adjusted arbitrarily, and has been tuned to the lowest cavity TE mode frequency. In the cylindrical resonator case this is the TE_{111} (or, for longer cavities, TE_{112}, TE_{113}, etc.) The closest in frequency background mode is TM_{011}, with frequency $f_{\mathrm{SG}} + \Delta f$.

There are two ways to discriminate against the background of direct charge excitation of the TM_{011} mode relative to the foreground MDM exitation of TE_{111} mode. The $\omega(\mathrm{TE}_{111})$ frequency is situated on the lower tail of the $\omega(\mathrm{TM}_{011})$ frequency response. Estimating the cavity Q-factors to be the same for both modes, this will reduce the background excitation at $\omega(\mathrm{TM}_{011})$ by one factor of $Q\Delta\omega/\omega_r$. The net background/foreground signal voltage ratio at ω_r would then be reduced by the same factor. With little control over $\Delta\omega$ this factor can only be maximized by increasing Q. There is also the possibility of damping the TM_{011} and higer modes relative to the TE_{111} mode, to reduce the higher mode excitation. But the benefit is less, since the damping also broadens the higher mode frequency spectrum.

Unfortunately, because the electron charge interaction is much greater than the magnetic moment interaction, the on-resonance response to beam charge at the TM_{011} mode frequency would be much greater than the on-resonance response to beam magnetization at the TE_{111} mode frequency. It is this huge ratio that needs to be overcome.

Reducing the sensitivity to direct charge excitation is pursued for rectangular resonators in the following section.

7.2. Estimation of skew penalty function $\mathcal{P}(\Theta)$. For calculating $\Delta\phi$ we proceed numerically, specializing to the TE_{202} case, with $\Theta = \tan^{-1} 1/2 = 26.565°$. Cavity fields for this case are shown in Figures 2 (c). The TE_{202} mode parameters are $(m, n, p) = (2, 0, 2)$, with $a = d$. It is convenient to scale spatial coordinates according to

$$\tilde{x} = \frac{\pi}{d}\, x, \quad y = 0, \quad \tilde{z} = \frac{\pi}{d}\, z, \quad K_c = \frac{2\pi}{a}. \tag{101}$$

Skew coordinates $(\tilde{x}', \tilde{z}')$ are related as in Figure 2 (b). With

$$\tilde{x} = \frac{2\pi}{a}\, x, \quad y = 0, \quad \tilde{z} = \frac{2\pi}{d}\, z, \tag{102}$$

the coordinate transformation is

$$\begin{aligned} \tilde{x} &= \cos\Theta\, \tilde{x}' - \sin\Theta\, \tilde{z}', \\ \tilde{z} &= \sin\Theta\, \tilde{x}' + \cos\Theta\, \tilde{z}'. \end{aligned} \tag{103}$$

Copying formulas from Conte[**2**], the field components are given by

$$\begin{aligned} \frac{B_x}{B_0} &= -\sin\tilde{x}\, \cos\tilde{z}\, \cos\omega t, \\ \frac{B_z}{B_0} &= \cos\tilde{x}\, \sin\tilde{z}\, \cos\omega t, \\ \frac{E_y}{B_0} &= \frac{\omega}{K_c}\, \sin\tilde{x}\, \sin\tilde{z}\, \sin\omega t, \end{aligned} \tag{104}$$

At the instant a particle enters the cavity at $(\tilde{x}, \tilde{z}) = (\pi/2, 0)$, traveling at speed V at angle Θ, as shown in Figure 2 (c), the phase of the horizontal magnetic field is zero by definition, meaning the magnetic arrow points right. At this instant,, at the eventual exit point $(\tilde{x}, \tilde{z}) = (-\pi/2, 2\pi)$, the phase is $\phi_I = -\pi$, meaning the horizontal magnetic field points left. (It would have been equivalent to have chosen the opposite sign for ϕ_I.)

On entry there is a longitudinal component of magnetic field $B_\parallel^{\text{entry}} = -B_0 \sin\Theta$. Our task is to find the longitudinal magnetic field $B_\parallel^{\text{exit}}$ at the instant the particle exits the cavity. The following equations are needed:

$$d = \lambda_g, \quad f = \frac{v_g}{\lambda_g} = \frac{\sqrt{2}\, c}{\lambda_g}, \quad L_V = \frac{\sqrt{5}}{2}\, \lambda_g, \quad t_V = \frac{L_V}{V} = \frac{\sqrt{5}}{2}\, \frac{d}{V}. \tag{105}$$

Here λ_g is the guide wavelength, $f = \omega/(2\pi)$ is the resonant frequency, L_V is the skew path length through the cavity, and t_V is the time of flight of the particle through the cavity. The wave exit phase is given by the starting phase at the exit point plus the cavity phase advance during the time t_V. This is also equal to the wave phase advance $\Delta\phi$. That is

$$\begin{aligned} \Delta\phi &= -\pi + 2\pi f t_V = -\pi + 2\pi \frac{\sqrt{2}\, c}{\lambda_g}\, \frac{\sqrt{5}}{2}\, \frac{\lambda_g}{V} = -\pi + 2\pi\sqrt{2}\, c\, \frac{\sqrt{5}}{2}\, \frac{1}{V} \\ &= \pi\Big(-1 + \frac{\sqrt{10}}{\beta_{_V}} \Big) \approx 2.16228\, \pi \equiv 0.16228\, \pi. \end{aligned} \tag{106}$$

We have taken $\beta_V = 1$ and, in the last line, subtracting 2π has no observable effect.

The role played by the resonant cavity is to carve out, from the passing waves, a slice of phase that acts on the particle. The worst possible slice would be any multiple of 2π, since there would be no net excitation in that case. This would be the case for $\Theta = 0$. This is why the path through the resonator has to be slanted. The best possible slice would be any odd multiple of π, which would give the maximumum

possible excitation. Quoted as a fraction of the maximum, in our case we have found $\Delta\phi/\pi = 0.16228$.

Unlike normal incidence to the cavity, for which input and output surfaces are permanent nodes and no net excitation possible, we are free to enter the cavity at arbitrary phase. But then the exiting phase is fixed. We should therefore enter the cavity at

$$\Phi_I^{\text{optimal}} = -\frac{\Delta\phi}{2} = 0.08114\,\pi. \tag{107}$$

It is actually the integral of a sinusoid rather than the phase angle that establishes the fractional excitation. Allowing for this we define a skew-entrance penalty $\mathcal{P}(\Theta)$ by

$$\mathcal{P}(\Theta) = \frac{\Delta\mathcal{E}}{\mathcal{E}^{\max}}(\Theta) = 2\sin\frac{\Delta\phi}{2}. \tag{108}$$

From this numerical example, for TE_{202}, we have found $\mathcal{P}(26.6^\circ) = 0.252$. The effect on Stern-Gerlach polarimetry is that, compared to direct electric excitation, transverse polarization is enhanced by a factor of $0.25\gamma_{\scriptscriptstyle V}^2$. Numerically, for GeV electrons, the enhancement factor is 500.

This is a respectable enhancement factor, but one can investigate other configurations to maximize the excitation. Repeating the same calculation in the case illustrated in Figure 2(a), with $\Theta = 45^\circ$ in a TE_{201} cavity. From equations like (104), the longitudinal magnetic field component along the skew axis is

$$\begin{aligned}\sqrt{2}B'_z &= (\cos\tilde{x}\sin\tilde{z} + \sin\tilde{x}\cos\tilde{z})\,\cos\omega t \\ &= \sin(\tilde{x}+\tilde{z}) = \sin(\sqrt{2}\tilde{x}')\,\cos\omega t.\end{aligned} \tag{109}$$

The longitudinal force is proportional to $\partial B'_z/\partial z$. But, according to this equation, B'_z is independent of z and the derivative vanishes. As a result the penalty function vanishes; $\mathcal{P}(45^\circ) = 0$. This is because the particle trajectory is parallel to two of the skew waves and perpendicular to the other two. Other attempts to increase $\mathcal{P}(\Theta)$ are considered later.

7.3. Estimation of background electric excitation. To estimate "background excitation we compare the expected MD excitations with the more familiar direct charge cavity excitation. After cancelling common factors, in the excitation ratios that have been derived so far, until the direct charge excitation term has been reduced to just the charge "e", then the longitudinal and transverse MD terms become "effective charges", and foreground/background ratios will be equal to these effective charges divided by e.

It has been the presence of the $\gamma_{\scriptscriptstyle V}^2$ factor in the third of Eqs. (84) that has made transverse Stern-Gerlach polarimetry seem especially promising. It is known from Eq. (66) that this factor gives the transverse magnetic moment a $\gamma_{\scriptscriptstyle V}$ advantage over longitudinal excitation. We have seen earlier that destructive interference makes this unduly optimistic, even fatal for on-axis beams through the resonator. Having partially suppressed the destructive interference by using a canted resonator, we continue the numerical foreground to background comparison.

As a first step to expressing these relations in MKS units the replacement $B_{0\|} = \mu_0 H_{0\|}$ has been made. The numerical value of μ_0 (which is *not* dimensionless) in MKS units is $4\pi \times 10^{-7}$Ṫ-m/A. For numerical evaluation it is then appropriate to intoduce "impedances" $Z_{\rm TM}$ and $Z_{\rm TE}$ given by

$$\begin{aligned} Z_{\rm TM} &= Z_0\sqrt{1 - f_c^2/f^2}, \\ Z_{\rm TE} &= \frac{Z_0}{\sqrt{1 - f_c^2/f^2}}, \\ \frac{Z_{\rm TM}}{Z_{\rm TE}} &= 1 - f_c^2/f^2. \end{aligned} \tag{110}$$

where $E = ZH$ and the value of "free space impedance" Z_0 is 377 V/A. Also

$$\cos\alpha_\pm = \pm\sqrt{1 - f_c^2/f^2}, \quad \text{and} \quad \sin\alpha_\pm = f_c/f. \tag{111}$$

Below Eq. (43) a typical value for the square root factor was said to be 0.5. For simplicity in producing a crude estimate, the square root factor can set to 1, causing the impedance factor to be just Z_0. For accurate calculations the frequency-dependent factors have to be restored.

8. Recapitulation and conclusions

As stated in the paper's first sentence, the essential conclusions have already been given in the first section. A new "skew wave" waveguide formalism, tailored to a canted resonator configuration has been introduced. Canting the resonator partially defeats the destructive interference that suppresses Stern-Gerlach resonant excitation for on-axis beam passage through the cavity. For conventional, on-axis, polarized beam, this formalism appears to be equivalent to that of Conte et al.[**2**].

To me the development of Stern-Gerlach polarimetry cannot be separated from the challenge of measuring the electric dipole moments (EDMs) of fundamental particles, (meaning electron, proton, and deuteron.) These measurements require exquisite, non-destructive, control of polarized beams in storage rings. Stern-Gerlach polarimetry is the only contemplated (much less proven) method of providing the necessary beam control.

The need for Stern-Gerlach polarimetry is most urgent in the electron case. With effective polarimetry the electron EDM measurement would be made relatively inexpensive by its relatively low, 15 MeV beam energy. But there is currently no form of electron polarimetry capable of providing the necessary beam control.

The situation is less unambiguous in the case of proton or deuteron EDMs. Quite well understood plans have been developed for measuring the proton EDM using beam control based on hadron-carbon scattering asymmetry. In time this form of polarimetry will permit the proton EDM to be measured, though possibly not at a level of precision sufficient to provide a stringent test of the standard model. Succesful Stern-Gerlach polarimetry can be expected to improve the accuracy of such proton (or deuteron) EDM measurements by an order of magnitude or more.

This paper has therefore been organized as a conservative development plan for developing Stern-Gerlach polarimetry, rather than as a most optimistic calculation of what the ultimate eventual polarimetry capability may be.

The obvious first step is to demonstrate the resonant excitation of a cavity by a polarized beam. Though first proposed 25 years ago this Stern-Gerlach effect has never been demonstrated experimentally. This failure can be partly ascribed to experimentalist's (fully-justified) timidity at attempting a very risky experiment and partly to a theorist's (correct) contention that the proposed experiment was guaranteed to fail. The only thing that has changed in the meantime is my introduction of slanted, off-axis passage of the polarized beam through the resonator. This re-establishes the original contention that the Stern-Gerlach force can be used to measure the polarization of a polarized beam, both non-destructively and with maximum analyzing power.

An ideal first test would use an ultra-high-Q superconducting cavity, with state-of-the-art instrumentation. This route could definitively test the principles at issue. But, regrettably, this route will be expensive and time consuming. This paper has therefore attempted to identify a first, inexpensive, room temperature test, with the potential of confirming the essential features of cavity excitation by Stern-Gerlach forces. Once proven at a rudimentary level, the further improvement of this form of polarimetry will be easy to justify.

The expense for room temperature cavity development for this proposed first test is minimal, and the required beam time to perform a proof-of-principle test will not be great. But the sacrifice in signal level and signal-to-noise ratio accompanying room temperature (as contrasted with low temperature) operation makes the calculated signal level all the more critical. I hope the formulas given in this paper are adequate to support planning of linac and/or storage ring tests. It is not obvious which route is more promising. Included in this uncertainty is the practicality and expense of producing the polarized beam needed to perform the first test. From my point of view this has become the dominant experimental uncertainty, and requires the most urgent study and development.

Equally urgent is theoretical confirmation that the slanted cavity approach does, in fact, overcome the strong tendency for destructive interference of Stern-Gerlach forces to suppress cavity excitation by a polarized beam.

I would like to thank Saul Teukolsky for helpful advice on this calculation.

Bibliography

[1] Ya. S. Derbenev, *RF-resonance beam polarimeter, Part I. Fundamental concepts,* Nuclear Instruments and Methods m Physics Research A 336, 12-15, 1993

[2] M. Conte, et al., *The Stern-Gerlach interaction between a traveling particle and a time varying magnetic field,* arXiv:physics/0003069v1 [physics.acc-ph], 2000

[3] P. Cameron, et al., *Proposal for a cavity polarimeter at MIT-Bates,* Proceedings of the Particle Accelerator Conference, Chicago, 2001

[4] C. Tschalaer, *Comment on the Paper "Stern-Gerlach Force in a Precessing Magnetic Moment,"*

[5] C. Tschalaer, *The Relativistic Stern-Gerlach Force,* arXiv/papers/0802/0802:0154.pdf, 2008

[6] C. Tschalaer, *Lorentz Transform of an Arbitrary Force Field on a Particle in its Rest Frame using the Hamilton-Lagrangian Formalism,* BIR#15-01, Bates Lab Report, 2015

[7] Y. Inoue, et al., *Development of a high-resolution cavity-beam position monitor,* PRST-AB **11**, 062801, 2008

[8] Siwon Jang et al., *Development of a cavity-type beam position monitor with high resolution for ATF2,* Proceedings of IPAC2013, Shanghai, China, 2013

[9] S. Ramo, J. Whinnery, and T. Van Duzer *Fields and Waves in Communication Electronics,* John Wiley, p. 467-470, 1965

[10] R. Talman, *Magnetic Resonance and Beam-Beam Polarimetry for Frozen Spin Storage Rings,* Report to Storage Ring EDM Collaboration, unpublished, 2012

[11] R. Talman, *Frequecy Domain Storage Ring for Electric Dipole Moment Measurement,* arXiv:physics/1508.04366 [physics.acc-ph], 2000

[12] M. Conte, et al., *Stern-Gerlach force on a precessing magnetic moment,* THPAS105, Proceedings of PAC07, Albuquerque, USA, 2007

[13] M. Conte, et al., *The Stern-Gerlach interaction between a traveling particle and a time varying magnetic field,* arXiv:0907.2161v1 [physics.acc-ph] 2009

[14] P. Cameron, et al., *An RF Resonance Polarimeter Phase I Proof of Principle Experiment,* RHIC/AP/126

[15] R. Talman and J. Talman, *ETEAPOT: symplectic orbit/spin tracking code for all-electric storage rings,* ArXiv:-phys.acc-phys:150308468, and submitted for publication to PRST-AB, 2015

[16] R. Talman and J. Talman, *Elecric dipole moment planning with a resurrected BNL Alternating Gradient electron analogue ring,* ArXiv:-phys.acc-phys:150308494, and submitted for publication to PRST-AB, 2015

[17] A. Kholmetskii, O. Missevitch, and T. Yarman, *Relativistic Transformation of Magnetic Dipole Moment,* Progress in Electromagnetics Research B, **47**, p.263-278, 2013

[18] J. Jackson, *Classical Electrodynamics,* 3rd edition, John Wiley, 1998

[19] R. Hagedorn, *Relativistic Kiematics,* W.A. Benjamin Inc., 1964

[20] P.C. Clemmons, *The Plane Wave Spectrum Representation of Electromagnetic Fields,* Institute of Electrical and Electronic Engineers, Inc., New York, Oxford University Press, 1996

[21] N. Marcuvitz, editor, *Waveguide Handbook,* McGraw Hill, 1951

[22] Ya. S Derbenev, *RF-resonance Beam Polarimeter", 11 th International Symposium on High Energy Spin Physics,* Bloomington, IN 1994, ISBN 1-56396- 374-4, AIP Conference Proceedings 343, 264-272, 1995

[23] P. R. Cameron et al., *Squids, Snakes, and Polarimeters: A New Technique for Measuring the Magnetic Moments of Polarized Beams*, Proceedings of the 1996 Beam Instrumentation Workshop, Argonne, 1996.
[24] Ya. S. Derbenev, *Radio-Frequency Polarimetry,* CP421, Polarized Gas Targets and Polarized Beams: Seventh International Workshop, edited by Roy J. Holt and Michael A. Miller, 1998 The American Institute of Physics, 1998
[25] Storage Ring EDM Collaboration, *A Proposal to Measure the Proton Electric Dipole Moment with* 10^{-29} *e-cm Sensitivity,* October, 2011

1. Appendices

1.1. Some magnetic dipole physical constants. The physical dimensions of magnetic moment μ^* are current times area, so its MKS units are A.m^2. Warnings have been given in the text that these physical units can be somewhat misleading when applied to the magnetic moment of a point particle, especially as regards transformation between reference frames. But, dimensionally, these are valid units for μ^*.) On the other hand, because $\mu^* B$ is an energy, μ^* can also be measured in MKS units of Joules/Tesla. Numerical values for various magnetic-moment related quantities are given for electron, proton, and deuteron, in Table 4.

TABLE 4. Electron, proton, and deuteron magnetic parameters. The units are SI, but with energies expressed in eV. Anomalous precession rates are in angular units of radians/second. The numbers are given to many-many places to indicate the accuracy to which the values are known. However, the actual values should not be trusted as authoratively correct to the accuracy they are shown here. In this paper, the scalar magnetic moment physical constants, μ_e, μ_p. μ_d, etc. are represented by the symbol μ^*.

	parameter	symbol	value	unit
	Bohr magneton	$\mu_B = e\hbar/(2m_e)$	$5.7883818066 \times 10^{-5}$	eV/T
e	g-factor	$g_e = 2\mu_e/\mu_B$	2.00231930436182	
	anomalous mag. mom.	$G_e = (\|g_e\| - 2)/2$	0.0011596521809	
	Larmor prec. rate	$g_e\mu_B/\hbar$	$-1.760859708 \times 10^{11}$	s^{-1}/T
	anom. precession rate	$G_e\mu_B/\hbar$	$1.019809775 \times 10^{8}$	s^{-1}/T
	nuclear magneton	$\mu_N = e\hbar/(2m_N)$	$3.1524512550 \times 10^{-8}$	eV/T
p	g-factor	$g_p = 2\mu_p/\mu_N$	5.585694702	
	anomalous mag. mom.	$G_p = g_p/2 - 1$	1.792847356	
	Larmor prec. rate	$g_p\mu_N/\hbar$	$2.675222005 \times 10^{8}$	s^{-1}/T
	anom. precession rate	$G_p\mu_N/\hbar$	0.859×10^{8}	s^{-1}/T
d	g-factor	$g_d = 2\mu_d/\mu_N$	0.8574382308	
	anomalous mag. mom.	$G_d = g_d - 1$	-0.14298	
	d/p mag. mom. ratio	μ_d/μ_d	0.3070122070	
	Larmor prec. rate	$g_d\mu_N/\hbar$	0.821325812	s^{-1}/T
	anom. precession rate	$G_d\mu_N/\hbar$	-0.6851×10^{7}	s^{-1}/T

2. Electromagnetic fields in low order resonant cavity modes

2.1. Resonator modes. The resonant polarimeter modes of choice will be TE rather than TM. Just as TM, because of its non-zero longitudinal electric field, is

needed for acceleration, TE is appropriate for resonant polarimetry because *TE modes do not accelerate*. Vanishing longitudinal electric field makes TE modes insensitive to beam charge. Equally important, their non-vanishing longitudinal magnetic fields make TE modes specially sensitive to magnetic moment excitation.

TE resonator modes are based on TE waveguide modes. The field patterns in two possible TE waveguide modes (TE_{01} and TE_{11}) are shown in Figure 11. The originally favored cylindrical mode was TE_{111}, shown on the right in this figure.

Cut-off frequencies for cylindrical waveguide modes are given in Table 9. It is important to remember that any cavity whatsoever has both TE and TM modes. What distinguishes a resonator as being TE is that it is being driven at a TE mode resonant frequency. Whatever the cavity shape, there are inevitably TM modes at not very remote frequencies. Resonant frequencies for a cavity having the favored pill-box shape, with definite length/radius (d/a) ratios, are given in Table 9. Absolute frequencies for a pill-box shaped cylindrical resonator with definite dimensions are given in Table 10. The entries in this table can be easily scaled, for example to lower frequencies, by increasing all dimensions proportionally.

It is now known that destructive interference for on-axis beam passage through the resonator favors rectangular resonators and pretty much rules out cylindrical resonators. The rectangular resonator mode most closely resembling cylindrical TE_{111}. Its fields are plotted in Figure 8.

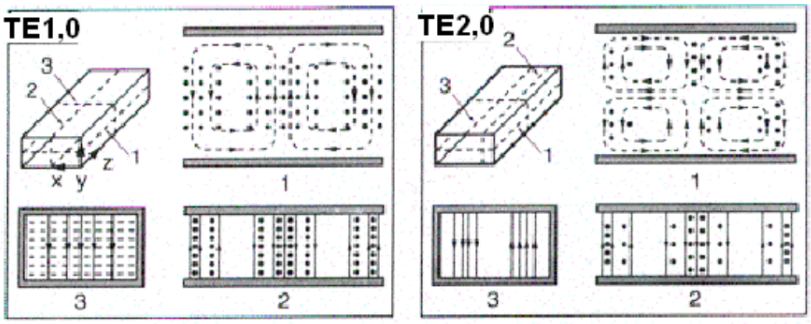

FIGURE 8. Field patterns for low order *rectangular* waveguide modes, TE_{10} and TE_{20}.

d/a	TM_{010}	TE_{111}	TM_{110}	TM_{011}	TE_{211}	TM_{111} TE_{011}	TE_{112}	TM_{210}	TM_{020}
0.00	1.00	∞	1.59	∞	∞	∞	∞	2.13	2.29
.50	1.00	2.72	1.59	2.80	2.90	3.06	5.27	2.13	2.29
1.00	1.00	1.50	1.59	1.63	1.80	2.05	2.72	2.13	2.29
2.00	1.00	1.00	1.59	1.19	1.42	1.72	1.50	2.13	2.29
3.00	1.13	1.00	1.80	1.24	1.52	1.87	1.32	2.41	2.60
4.00	1.20	1.00	1.91	1.27	1.57	1.96	1.20	2.56	3.00
∞	1.31	1.00	2.08	1.31	1.66	2.08	1.00	2.78	3.00

FIGURE 9. Resonant frequencies of *cylindrical* resonator modes as a function of length/radius=d/a.

TE

n	m	p	f (GHz)
1	1	1	2.016756
1	1	2	2.513305
2	1	1	3.14312
1	1	3	3.172648
2	1	2	3.482614

TM

n	m	p	f (GHz)
0	1	0	2.379399
0	1	1	2.532062
0	1	2	2.942912
0	1	3	3.522744
1	1	1	3.888838

FIGURE 10. *Cylindrical* resonator mode frequencies for a special case, a=4.826 cm, d=17.323 cm, d/a=3.59. As required, the lowest frequency mode is TE, and the closest TM mode is well separated. For lower frequency modes the dimensions would be proportionally greater.

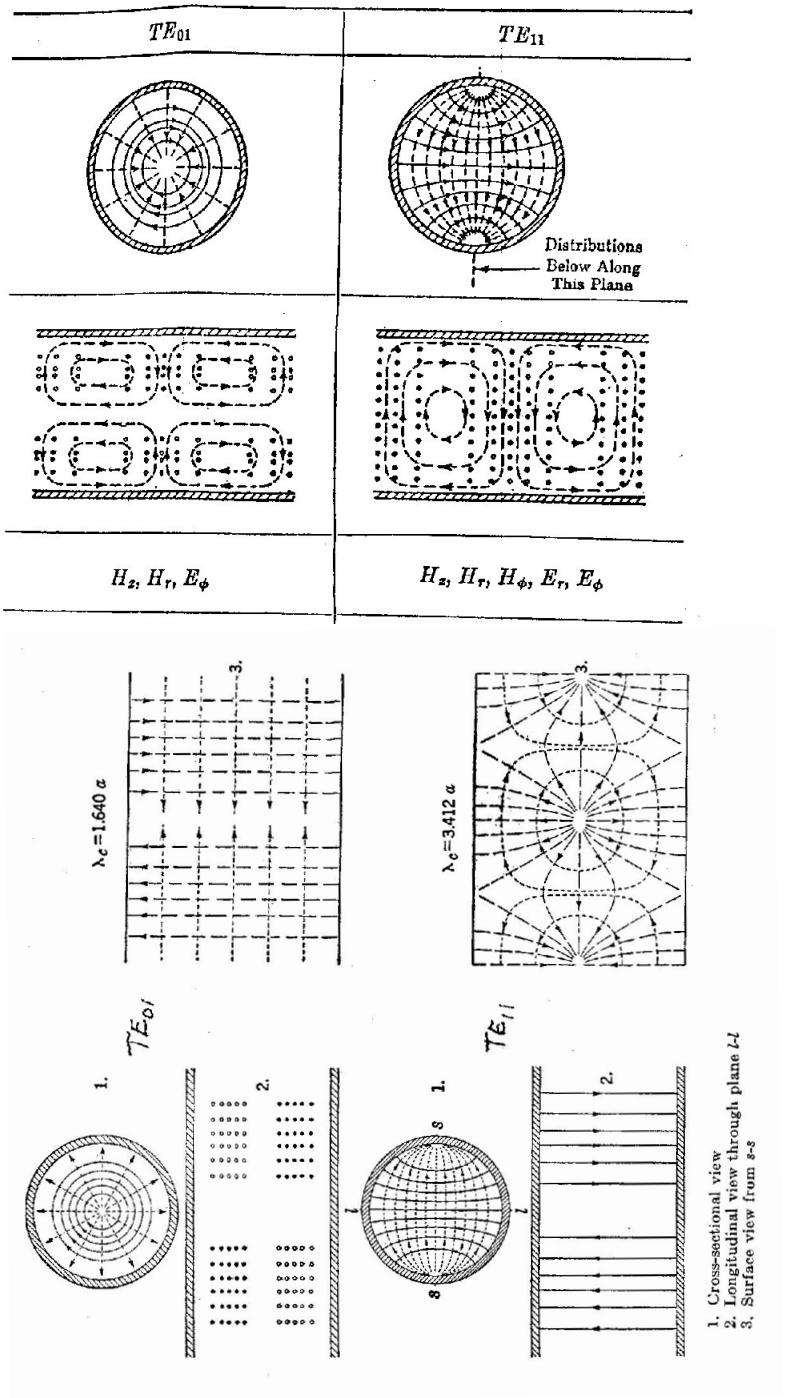

FIGURE 11. Various views of the electric and magnetic lines in promising *cylindrical* modes, Ramo et al.[**9**] above, and Waveguide Handbook[**21**] below. TE_{01} on the left, TE_{11} on the right. Solid lines and dots are electric fields. Broken lines are magnetic fields (different spacing for different magnetic components).